Journal of the Mechanics and Physics of Solids 60 (2012) 1883–1906

Contents lists available at SciVerse ScienceDirect

Journal of the Mechanics and Physics of Solids

journal homepage: www.elsevier.com/locate/jmps

Driving forces in moving-contact problems of dynamic elasticity: Indentation, wedging and free sliding

Leonid I. Slepyan [a,*], Michele Brun [b,c]

[a] School of Mechanical Engineering, Tel Aviv University, P.O. Box 39040, Ramat Aviv 69978 Tel Aviv, Israel
[b] Dipartimento di Ingegneria Meccanica, Chimica e dei Materiali, Universitá di Cagliari, Piazza d'Armi, I-09123 Cagliari, Italy
[c] Istituto Officina dei Materiali del CNR (CNR-IOM) Unitá SLACS, Cittadella Universitaria, 09042 Monserrato (Ca), Italy

ARTICLE INFO

Article history:
Received 14 March 2012
Received in revised form
18 June 2012
Accepted 29 June 2012
Available online 10 July 2012

Keywords:
Dynamics
Contact mechanics
Analytic functions
Moving indentation
Wedging

ABSTRACT

The steady-state solution for an elastic half-plane under a moving frictionless smooth indenter of arbitrary shape is derived based on the corresponding transient problem and on a condition concerning energy fluxes. Resulting stresses and displacements are found explicitly starting from their expressions in terms of a single analytical function. This solution incorporates all speed ranges, including the super-Rayleigh subsonic and intersonic speed regimes, which received no final description to date. Next, under a similar formulation the wedging of an elastic plane is considered for a finite wedge moving at a distance from the crack tip. Finally, we solve the problem for such a wedge moving along the interface of two elastic half-planes compressed together. Considering these problems we determine the driving forces caused by the main underlying factors: the stress field singular points on the contact area (super-Rayleigh subsonic speed regime), the wave radiation (intersonic and supersonic regimes) and the fracture resistance (wedging problem). In addition to the sub-Rayleigh speed regime, where the sliding contact itself gives no contribution to the driving forces, there exists a sharp decrease in the resistance in the vicinity of the longitudinal wave speed with zero limit at this speed.

1. Introduction

For potential flow of unbounded incompressible perfect fluid d'Alembert proved that *the solid body moving with constant velocity meets zero drag force* (see, e.g., Darrigol, 2002). This follows from the Laplace equation as a highly simplified mathematical model of fluid dynamic. At the same time, this 'paradox' has more wide underlying physics. In particular, it can be met in elasticity, which is also an appropriate model. By comparing and considering the viscosity and instability of potential flow of fluid, the elasticity looks even more adequate.

For example, we can consider a smooth indenter uniformly moving without friction along an elastic half-plane boundary or along an infinite layer rested on a rigid foundation. Of course, contrary to fluids, a macroscopic rigid body can move *through* an intact elastic medium only if the movement is accompanied by fracture, that creates resistance to the movement. In this case, the question remains as whether the contact interaction itself gives a contribution to the resistance in addition to the fracture resistance alone.

* Corresponding author. Tel.: +972 3640 6224; fax: +972 3640 7617.
E-mail address: leonid@eng.tau.ac.il (L.I. Slepyan).

0022-5096/$ - see front matter © 2012 Elsevier Ltd. All rights reserved.
http://dx.doi.org/10.1016/j.jmps.2012.06.011

So, under certain conditions, the d'Alembert's statement remains valid in more general steady-state cases. Namely, it can be true with respect to any medium or structure, where such regime can exist, if no energy can be dissipated or released in the medium in which the body moves, in the contact zones, in other boundaries, if exist, and at infinity. In other words, this means that (a) the medium and the boundaries are perfect, (b) no singular points exist at which the energy can be dissipated or released, including such point at infinity, that is, no configurational and remote forces exist , and (c) there are no waves which could carry the energy away from the body or to the body. Since no energy is radiated or absorbed while in motion, no driving force is required to support the steady-state regime. In the present paper, we assume the strains to be sufficiently small so that strain-associated thermal effects can be neglected. Along with the 'paradoxical' regimes, we study in detail the others, where driving forces arise caused by singular points, wave radiation and fracture resistance.

It can happen that a couple of singular points exists, one of them, the *energy-source point* radiates energy, while the other, the *energy absorbing point* absorbs the radiated energy. In this energy-balance case, the regime might be considered as a free motion, which does not require any driving force. This, however, could be true if the energy-source point is physically justified as a real 'micro-level' source. Otherwise, the energy-source point must be eliminated. This consideration has a crucial importance for the super-Rayleigh subsonic speed regime. An indenter uniformly moving along the elastic half-plane boundary with subsonic speeds (except the Rayleigh wave speed) excites no wave. Thus, in this speed range, only the existence of friction or/and energy-flux-significant singular points can prohibit *d'Alembert's paradox*. Such singular points really appear at the super-Rayleigh subsonic speeds. This also concerns the movement of a body along the interface between two elastic half-planes compressed together.

The steady-state dynamic contact problem was repeatedly considered. In particular, the problem for a parabolic indenter was considered by Craggs and Roberts (1967), Georgiadis and Barber (1993), Brock (2002) and in Galin and Gladwell (2008). While the problem for the sub-Rayleigh speed range received the complete solution, the super-Rayleigh sub- and intersonic regimes are still under question. These regimes were discussed in Georgiadis and Barber (1993) and Brock (2002), where no way was found how to make the solutions to be unique and/or physically accepted. Note that dynamic problems for straight-propagating cracks are closely related to the dynamic contact problems. The super-critical regimes for cracks are considered in many works, mainly for mode II shear fracture, see, e.g., Freund (1990), Huang et al. (1998), Broberg (1999), Needleman (1999), Gao et al. (2001), Geubelle and Kubair (2001), Samudrala et al. (2002) and Slepyan (2002). Mode I opening crack, intersonic speed problem was considered by Radi and Loret (2008) for a porous, liquid-saturated material, where, however, 'intersonic' does not mean the shear–longitudinal range in the uniform solid material considered below.

The above-mentioned nonuniqueness suggests that there is a missed point in the problem formulation. In this connection, in addition to the well-known Signorini contact conditions, we add the condition concerning the energy-flux significant singular points in the stress–particle velocity field: no energy-source singular point can exist, as a source of energy, unless such a point source is physically justified. Thus, we base our solutions on the following three conditions:

(a) positive (tensile) normal contact stresses are not allowed,

(b) penetration of the elastic material into the indenter is not allowed,

(c) energy-source singular points are not allowed. (1)

With respect to the latter condition we note that an angular point of the body surface can give rise of an energy absorbing singular point. In the super-Rayleigh speed regimes, singular points arise in the case of a smooth body shape as well. As an example of energy-transfer singular point a moving semi-infinite crack can be considered. Under sub-Rayleigh speeds the crack tip appears to be an energy absorbing singular point. In the hypothetic case of super-Rayleigh subsonic speeds, the crack tip is an energy source. Usually, there is no such source in the elastic material, and if the crack tip is free of external actions, this regime is impossible. However, if a hypothetic tool exists, which can act directly on the crack tip just giving the required energy, the super-Rayleigh crack speed seems to be possible. In any case, the semi-infinite crack growth requires external energy.

In the case of the Yoffe (1951) model of the propagating constant-length crack, there are two singularities, the front and the rear end points of the crack. For sub-Rayleigh speeds the former is the energy absorber, while the latter is the energy source. The energy radiated by the rear point goes to the front point and thereby supports the crack movement. A body embedded inside the crack can thus move freely together with the crack. Is this the 'paradox' manifestation? It would be so if there was a sort of 'channel' through which the energy could be transferred from one point to the other. Otherwise, a real source of energy must exist at the rear point to support the process, that is, a nonzero driving force must exist. In any case, if no such energy source is assumed, the formal solution for the moving finite-length crack cannot be accepted. Nevertheless, a configuration like a propagating constant-length crack can exist as a finite separation zone between two elastic half-planes, or two layers, which are compressed together. Such 'nonsingular' moving zone was considered with respect to a different problem by Comninou and Dundurs (1977).

The above-mentioned three conditions (1) are sufficient for the half-plane contact problem, and the solutions, obtained here for a smooth frictionless contact area moving at any speed, are uniquely defined. In the super-Rayleigh subsonic speed range, the leading point of the contact area appears as an energy absorbing singular point. Thus, a speed-dependent driving force is required for the motion. In the intersonic and supersonic speed regimes, the wave radiation creates resistance.

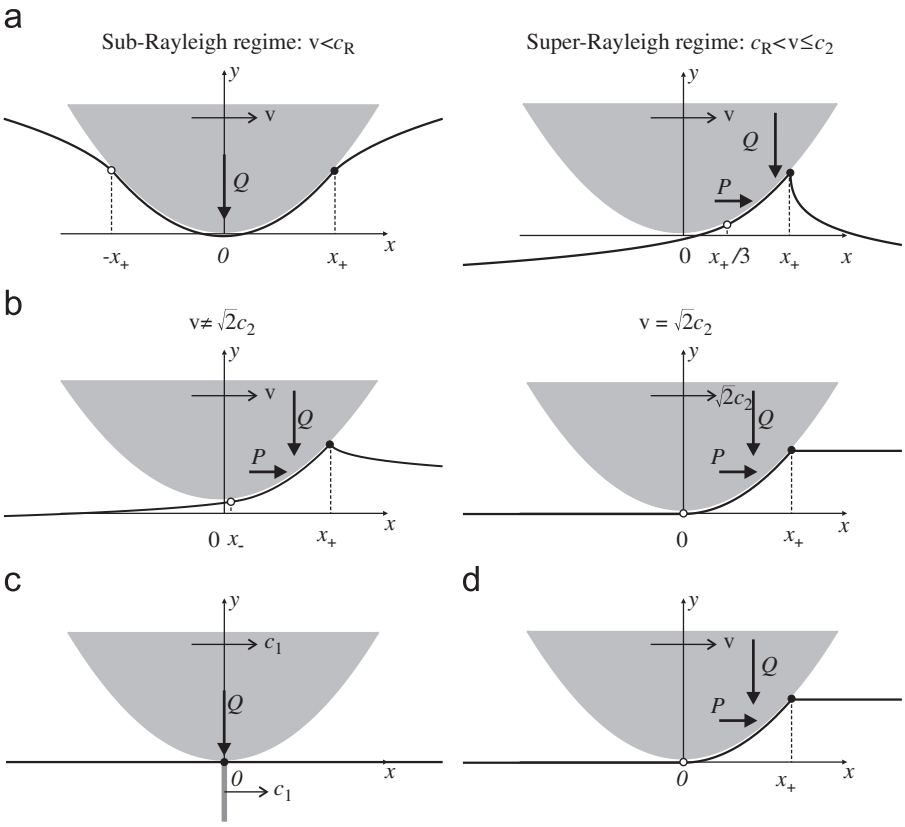

Fig. 1. The contact configurations in different speed regimes (Section 3). The bold curve is the deformed elastic half-plane boundary. The leading, x_+, and the rear, x_-, end points of the contact region are marked by black and white circles, respectively. In this figure, notation x is used instead of η as accepted below beginning from Section 2.3. The localized longitudinal wave in equilibrium with the indenter is sketched in (c). (a) Subsonic regime: $v \le c_2$. (b) Intersonic regime: $c_2 \le v < c_1$. (c) Longitudinal wave speed: $v = c_1$. (d) Supersonic regime: $v > c_1$.

The contact configurations for the sub- and super-Rayleigh subsonic, intersonic and supersonic speed regimes can be compared in Fig. 1, where we anticipate the results of Section 3. It is of interest that not only for subsonic speeds but also for the longitudinal wave speed there is no resistance to the movement in the steady-state regime.

Besides the half-plane contact problem, the related problem of the steady-state wedging of an elastic plane by a smooth rigid body is investigated below. This problem for sub- and super-Rayleigh speeds was considered by Barenblatt and Cherepanov (1960) and Barenblatt and Goldstein (1972), respectively. In the former work, a semi-infinite, 'moving-with-friction' rigid wedge placed at a distance from the crack tip was considered, while in the latter a finite-length, 'moving-without-friction' wedge in contact with the crack tip was analyzed, and condition (a) in (1) was used. In both cases, only one simply connected stress-free region was present in the problem formulation. Here, we consider this problem for a finite-length wedge placed at a distance from the crack tip. In this case, there are two stress-free regions, and the problem appears more complicated but analytically solvable. The obtained solution presents relations between all the input and output quantities: the fracture resistance, the wedge shape and width and the driving force (or the speed), on one hand, and the wedge/crack speed (or the driving force), the wedge position, the contact area and the contact stress distribution, on the other.

We also consider the movement of a finite rigid body along the interface of two elastic half-planes compressed together, where no energy significant singularities exist at sub-Rayleigh speeds. The paper by Comninou and Dundurs (1977) prompted the authors to address this problem.

The steady-state solution of these problems is preceded by the analysis of the transient problem for a normal load moving along the elastic half-plane boundary. We construct the solution corresponding to the load distributed as a pre-delta function that results in a more transparent solution, with the corresponding Green's function as a limit. Then we derive the steady-state limit and the asymptotic representations. The transient solution allows us to extract explicitly the general expressions of the normal traction and the derivative of the displacement trough a single analytical function. These expressions valid for all ranges of the speed are then used to address the above-mentioned mixed problems. The use of the transient problem with zero initial conditions also allows us to exclude automatically the energy flux from infinity, which is important for intersonic and supersonic regimes.

The problems are considered in the framework of linear isotropic elasticity. This implies that strains and rotations are assumed to be small enough, and contact normal stresses can be considered as a true traction, σ_{yy}, acting on the half-plane boundary. Mathematically, the considered mixed problems are formulated and solved (a) for a single region where the real part of an analytical function is given, whereas the imaginary part of this function is given outside of this region

(the dynamic contact problem for the half-plane), (b) for two such regions (the wedging problem for the elastic plane) and (c) for three regions (the two half-planes compressed together). Note that the analytical technique used in this paper is applicable for any number of the 'real-part' regions and for a periodic array of the real/imaginary (stress/displacement) regions. So the considered problems can also be solved, in the same way, for the contact zone consisting of several simply connected regions or of a periodic array of such regions.

In the wedging problem a driving force is required to force the crack to grow as it should be. However, in the sub-Rayleigh speed regime, the driving force is just equal to the crack resistance; the contact interaction gives no additional contribution to the driving force. At Rayleigh wave speed c_R there is no steady-state solution of the half-plane problem. In this resonant regime, the displacement grows in proportion to time if a constant vertical force is given, or the contact stresses rapidly vanish in time if a constant vertical displacement of the indenter is given. For the super-Rayleigh subsonic speeds, $c_R<v\le c_2$, there is energy release though a singular point at the front end of the contact zone. In this case, a driving force is required to support the motion. It can be equally treated as a Newtonian force or as a configurational force of the same power (as in the case where the indenter is a self-propelled body):

$$P=-\int_{x_-}^{x_+}\sigma_{yy}(x)u_y'(x)\,\mathrm{d}x=\frac{1}{v}\int_{x_-}^{x_+}\sigma_{yy}(x)\dot{u}_y(x)\,\mathrm{d}x, \tag{2}$$

respectively, where $[x_-,x_+]$ is the contact segment and the equality follows from the fact that, in the steady-state regime, $\partial u_y/\partial t=-v\partial u_y/\partial x$. Note that the first equality is valid for the transient regime too. Indeed, let the half-plane boundary be defined as $y(x,t)$. The partial t-derivative, $\partial y(x,t)/\partial t$, corresponds to a given point on the half-plane boundary, whereas the 'total' derivative, $\mathrm{d}y(x(t),t)/\mathrm{d}t$, corresponds to the vertical speed of the rigid body moving with horizontal speed $v(t)=\mathrm{d}x(t)/\mathrm{d}t$. The latter derivative, the work rate due to the vertical movement of the body, N_Q, and the total rate of the work, N, are

$$\frac{\mathrm{d}y(x(t),t)}{\mathrm{d}t}=\frac{\partial y(x,t)}{\partial t}+v(t)\frac{\partial y(x,t)}{\partial x},$$
$$N_Q=-\int_{x_-}^{x_+}\sigma_{yy}(x,t)\frac{\mathrm{d}y(x(t),t)}{\mathrm{d}t}\mathrm{d}x,\quad N=-\int_{x_-}^{x_+}\sigma_{yy}(x,t)\frac{\partial y(x,t)}{\partial t}\mathrm{d}x \tag{3}$$

and the driving force is

$$P=-\frac{N-N_Q}{v(t)}=-\int_{x_-}^{x_+}\sigma_{yy}(x,t)\frac{\partial y(x,t)}{\partial x}\mathrm{d}x. \tag{4}$$

(Green's function for the latter derivative is presented in (19).)

In the intersonic regime, $c_2<v<c_1$, the singular point becomes weaker, it can neither absorb nor release energy; however, a shear wave arises which carries energy from the indenter. At a special speed, $v=c_2\sqrt{2}$, the field is represented by this wave only. It is the speed of the point of intersection of the x-axis with the wave front tilted at an angle of 45°. In this orientation, the shear wave is supported by the normal pressure, $\sigma_{yy}(x)$, only, and no other field can arise. This is why the half-plane outside of the wave, $x-y<x_-,x-y>x_+$, remains at rest (with a shift of the displacement). Note that by the same reason no wave is excited in the case of a tangential action, which could be referred to mode II symmetry. In the supersonic case, $v>c_1$, both the shear wave and the longitudinal wave are radiated.

Note that the body–elastic half-plane interaction at these speeds, $v=\sqrt{2}c_2$ and $v>c_1$, resembles the aquaplaning, and this is not a coincidence: these are similar wave phenomena.

Lastly, at the longitudinal wave speed limit the resistance appears equal to zero with a sharp decrease in the vicinity of this speed. In this limit, only a localized longitudinal wave exists in the half-plain, in equilibrium with the indenter. This is a special example where no driving force is needed to sustain the motion.

2. Transient problem for a moving load

First we consider the transient problem corresponding to zero initial conditions. The solution will allow us to predict possible steady-state regimes, to extract the steady-state limits, if exist, and to see the transient process otherwise.

2.1. General solution

Consider an elastic half-plane, $-\infty<x<\infty$, $y<0$, initially at rest and subjected at $t=0$ to a hereafter invariable normal load uniformly moving along the x-axis. The load can be represented as

$$\sigma_{yy}(x,t)=\sigma(\eta)H(t),\quad \eta=x-vt,\ v=\mathrm{const}, \tag{5}$$

where H is the Heaviside step function. In the following we use the Fourier transform on x $((.)^F)$ and on η $((.)^{F_\eta})$, and the Laplace transform on time, t $((.)^L)$. Note that in these terms

$$\sigma_{yy}^{LF}(k,s)=\int_{-\infty}^{\infty}\int_0^{\infty}\sigma_{yy}(x,t)\mathrm{e}^{\mathrm{i}kx-st}\,\mathrm{d}t\,\mathrm{d}x=\frac{\sigma^{F_\eta}(k)}{s-\mathrm{i}kv},$$

$$\sigma^{F_\eta}(k)=\int_{-\infty}^{\infty}\sigma(\eta)\mathrm{e}^{\mathrm{i}k\eta}\,\mathrm{d}\eta. \tag{6}$$

To avoid singularities and thus to make the corresponding Green's function more transparent we choose the load to be distributed as a regular pre-delta function, namely

$$\sigma(\eta)=\frac{\varepsilon Q_y}{\pi(\eta^2+\varepsilon^2)}\to Q_y\delta(\eta)\ (\varepsilon\to 0),\quad \sigma^{F_\eta}(k)=Q_y\mathrm{e}^{-\varepsilon|k|}\ (\Im k=0,\ \varepsilon>0), \tag{7}$$

where the constant $Q_y=-Q$ ($Q\ge 0$) is the total force. Note that in the plane problem the dimension of Q is N/m.

The Laplace and Fourier, *LF*-transform of the prelimiting Green's function (multiplied by Q_y) for the normal particle velocity at $y=0$ is (see, e.g., Slepyan, 2002, p. 300)

$$(\dot u_y)^{LF}(k,s)=G_\varepsilon^{LF}(k,s)=\frac{s^3n_1}{c_2^2\mu R_n}\sigma_{yy}^{LF}(k,s)=\frac{Q_ys^3n_1\mathrm{e}^{-\varepsilon|k|}}{c_2^2(s-\mathrm{i}k\nu)\mu R_n}, \tag{8}$$

where

$$R_n=(k^2+n_2^2)^2-4k^2n_1n_2,\quad n_{1,2}=\sqrt{k^2+s^2/c_{1,2}^2} \tag{9}$$

and the longitudinal and shear wave speeds are

$$c_1=\sqrt{(\lambda+2\mu)/\varrho},\quad c_2=\sqrt{\mu/\varrho}, \tag{10}$$

respectively, with λ,μ the Lamé elastic constants and ϱ the mass density. In addition to these waves, an important role is played by the Rayleigh surface wave. Its speed, $c_R<c_2$, is defined by $R(c_R)=0$, in which the Rayleigh function

$$\begin{aligned}R(\nu)&=(1+\alpha_2^2(\nu))^2-4\alpha_1(\nu)\alpha_2(\nu),\quad \alpha_{1,2}=\sqrt{1-\nu^2/c_{1,2}^2}\ (0<\nu<c_2),\\&=(1-\beta_2^2(\nu))^2+4\mathrm{i}\alpha_1(\nu)\beta_2(\nu),\quad \beta_2=\sqrt{\nu^2/c_2^2-1}=\mathrm{i}\alpha_2\ (c_2<\nu<c_1),\\&=(1-\beta_2^2(\nu))^2+4\beta_1(\nu)\beta_2(\nu),\quad \beta_1=\sqrt{\nu^2/c_1^2-1}=\mathrm{i}\alpha_1\ (\nu>c_1).\end{aligned} \tag{11}$$

Expression (8) satisfies the conditions which allow the original expression for function $G_\varepsilon(x,t)$ to be obtained using the Cagniard–de Hoop method, Cagniard (1962) and De Hoop (1959). A modified version of this method, which does not require any transformation of the integration path, was presented in Slepyan (1972, pp. 80–85; 2002, pp. 61–63), where the result was derived explicitly for a general case. Here, for the convenience of the reader, we do not use the final result but the method itself in its application to the considered double transform.

First, we introduce parameter q by equality $k=qs$, assuming $s>0$. We now have $\mathrm{d}k=s\,\mathrm{d}q$ and

$$\begin{aligned}&G_\varepsilon^{LF}(k,s)=\frac{Q_y}{s}f(q)\mathrm{e}^{-\varepsilon s|q|},\quad f(q)=\frac{m_1}{c_2^2\mu(1-\mathrm{i}q\nu)R_m(q)},\\&R_m(q)=(2q^2+1/c_2^2)^2-4q^2m_1m_2,\quad m_{1,2}=\sqrt{q^2+1/c_{1,2}^2}.\end{aligned} \tag{12}$$

Next, we represent *L*-transform of Green's function as the generalized inverse Fourier transform

$$\begin{aligned}&G_\varepsilon^L(z,s)=\frac{Q_y}{2\pi}\left[\lim_{z\to-\mathrm{i}x}G_{\varepsilon+}^L(z,s)+\lim_{z\to\mathrm{i}x}G_{\varepsilon-}^L(z,s)\right],\\&G_{\varepsilon+}^L(z,s)=\int_{-\infty}^{0}f(q)\mathrm{e}^{(\varepsilon+z)sq}\,\mathrm{d}q=\int_0^{\infty}f(-q)\mathrm{e}^{-(\varepsilon+z)sq}\,\mathrm{d}q\ (\Re z>0),\\&G_{\varepsilon-}^L(z,s)=\int_0^{\infty}f(q)\mathrm{e}^{-(\varepsilon+z)sq}\,\mathrm{d}q\ (\Re z>0).\end{aligned} \tag{13}$$

In the third step, we substitute $q(\varepsilon+z)=t$, assuming for the moment that z lies on the real positive half-axis, $z>0$. This yields

$$\begin{aligned}&G_{\varepsilon+}^L(z,s)=\frac{1}{\varepsilon+z}\int_0^{\infty}f(-t/(\varepsilon+z))\mathrm{e}^{-st}\,\mathrm{d}t,\\&G_{\varepsilon-}^L(z,s)=\frac{1}{\varepsilon+z}\int_0^{\infty}f(t/(\varepsilon+z))\mathrm{e}^{-st}\mathrm{d}t.\end{aligned} \tag{14}$$

Further, since each of the integrals represent the Laplace transform, it follows that

$$G_{\varepsilon\pm}(z,t)=\frac{m_1}{c_2^2\mu(\varepsilon+z)(1\pm\mathrm{i}q\nu)R_m(q)}. \tag{15}$$

Now, in accordance with the generalized Fourier transform, we make analytical continuation from $z>0$ to the imaginary axis, $z\to \mp \mathrm{i}x$ for $G_{\varepsilon\pm}(z,t)$, respectively. We obtain

$$G_\varepsilon(z,t)=\frac{Q_y}{2\pi}\left[\lim_{z\to -\mathrm{i}x} G_{\varepsilon+}(z,t)+\lim_{z\to \mathrm{i}x} G_{\varepsilon-}(z,t)\right], \tag{16}$$

with

$$q=\pm\frac{\mathrm{i}t}{x\pm\mathrm{i}\varepsilon},\quad m_{1,2}=\pm\frac{\mathrm{i}t}{x\pm\mathrm{i}\varepsilon}\alpha_{1,2},\quad (1\pm\mathrm{i}qv)=1-\frac{vt}{x\pm\mathrm{i}\varepsilon},$$
$$R_m=\frac{t^4}{(x\pm\mathrm{i}\varepsilon)^4}R((x\pm\mathrm{i}\varepsilon)/t), \tag{17}$$

where symbol $\pm$ corresponds to $G_{\varepsilon\pm}(z,t)$, respectively.

Finally, referring to (12) and (15) we obtain

$$G_\varepsilon(x,t)=\dot u_y(x,t)=\frac{Q_y}{\pi}\Re\left[\lim_{z\to -\mathrm{i}x} G_{\varepsilon+}(z,t)\right]=-\frac{Q_y}{\pi\mu c_2^2 t^3}\Re\left[\frac{(x+\mathrm{i}\varepsilon)^3\sqrt{1-(x+\mathrm{i}\varepsilon)^2/(c_1t)^2}}{(x-vt+\mathrm{i}\varepsilon)R[(x+\mathrm{i}\varepsilon)/t]}\right]. \tag{18}$$

This fundamental relation between the stress and the time-derivative of the displacement is valid for any speed, v. Below it is extended by superposition for an arbitrary stress distribution and used in the formulation of the contact problems. Note that this technique is valid for the determination of the field for $y<0$ as well as for $y=0$. We recall that Green's function itself is the limit of $G_\varepsilon(x,t)$ $(\varepsilon\to+0)$.

Green's functions corresponding the displacement and its x-derivative follow from (18) as

$$G_u(x,t)=-\frac{Q_y}{\pi\mu c_2^2}\Re\int_{x/t}^{\infty}\frac{\xi^2\sqrt{1-\xi^2/c_1^2}}{(\xi-v)R(\xi)}\mathrm{d}\xi\quad\left(\xi=\lim_{\varepsilon\to+0}\xi+\mathrm{i}\varepsilon\right),$$
$$\frac{\partial G_u(x,t)}{\partial x}=\frac{Q_y}{\pi\mu c_2^2}\Re\frac{(x/t)^2\sqrt{1-(x/c_1t)^2}}{(x-vt)R(x/t)}\quad\left(x=\lim_{\varepsilon\to+0}x+\mathrm{i}\varepsilon\right). \tag{19}$$

2.2. The steady-state limits and the asymptotic representations

2.2.1. The limits

The steady-state limit, if exists, follows from (18) with $\varepsilon>0$ as

$$\lim G_\varepsilon(vt+\eta,t)=G_\varepsilon(\eta)=\dot u_y(\eta)=-vu_y'(\eta)=-\frac{Q_y v^3}{\pi\mu c_2^2}\Re\left[\frac{\sqrt{1-v^2/c_1^2-\mathrm{i}0}}{(\eta+\mathrm{i}\varepsilon)R(v-\mathrm{i}0)}\right]\quad(t\to\infty,\ \eta/t\to0). \tag{20}$$

For the subsonic speed regime, including the shear wave speed and except the Rayleigh wave speed, c_R, it follows that

$$G_\varepsilon(\eta)=-\frac{Q_y v^3\alpha_1(v)}{\pi\mu c_2^2R(v)}\frac{\eta}{\eta^2+\varepsilon^2}\quad(0<v<c_R,\ c_R<v\le c_2). \tag{21}$$

In this speed regime, there is no limit for the displacement.

For the intersonic speed region, $c_2\le v\le c_1$, we have

$$G_\varepsilon(\eta)=-\frac{Q_y v^3\alpha_1(v)}{\pi\mu c_2^2}\frac{(1+\alpha_2^2(v))^2\eta-4\alpha_1(v)\beta_2\varepsilon}{(1+\alpha_2^2(v))^4+16\alpha_1^2(v)\beta_2^2(v)}\frac{1}{\eta^2+\varepsilon^2}. \tag{22}$$

Finally, for the supersonic regime, $v\ge c_1$,

$$G_\varepsilon(\eta)=\frac{Q_y v^3}{\pi\mu c_2^3}\frac{\beta_1(v)}{(1+\alpha_2^2(v))^2+4\beta_1(v)\beta_2(v)}\frac{\varepsilon}{\eta^2+\varepsilon^2}. \tag{23}$$

2.2.2. The asymptotic representations

There are two special rays in this problem: $x=c_Rt$ and $x=c_1t$, where there is no steady-state limit for $\varepsilon\ge0$ and for $\varepsilon=0$, respectively. For these cases we consider the asymptotic representations, $t\to\infty$, for the particle velocities and for the displacements. Also we consider the asymptotic difference between the transient and the corresponding steady-state limit for some cases where the latter exists. From the solution (18) it follows that

$$G_\varepsilon\sim-\frac{Q_y c^3\alpha_1}{\pi\mu c_2^2(c-v)R(c)t}\quad(x=ct\ne vt,\ 0<c<c_2,\ c\ne c_R),$$

$$G_\varepsilon \sim -\frac{Q_y}{\pi\mu c_2^2}(U_\eta + U_t) \quad (x = vt+\eta,\ c_2 > v \neq c_R),$$

$$U_\eta = \frac{v^3\alpha_1}{R(v)}\frac{\eta}{\eta^2+\varepsilon^2}, \quad U_t = \frac{v^2\alpha_1}{R(v)t}\left(3-\frac{v^2}{c_1^2\alpha_1^2}-\frac{vR'(v)}{R(v)}\right), \tag{24}$$

with

$$R'(v) = \frac{\mathrm{d}R(v)}{\mathrm{d}v} = \frac{4v}{c_2^2}\left(\frac{c_2^2\alpha_2}{c_1^2\alpha_1}+\frac{\alpha_1}{\alpha_2}-1-\alpha_2^2\right). \tag{25}$$

The latter asymptotic representation consists of two very different terms. In the moving coordinate system, the first term, $U_\eta = U_\eta(v,\eta)$, is independent of time; it corresponds to the steady-state regime. This term is orthogonal to the load and the corresponding rate of the work and hence the driving force is zero. Indeed, for sub-Rayleigh speeds, the load is symmetric but the particle velocities are antisymmetric. Note that this statement concerning the driving force is still valid for the contact stress distribution corresponding to a smooth indenter of an arbitrary shape (see Section 3.2.1).

The second term, $U_t = U_t(v,t)$, is asymptotically independent of the coordinate but depends on time. It corresponds to the subsidence of the elastic half-plane under the load. Contrary to the former the latter has the same signum in both sub-Rayleigh and super-Rayleigh subsonic regimes; namely, $U_t < 0$ ($0 < v < c_R$, $c_R < v < c_2$). Besides, it is symmetric, and the load does work on this vertical motion. There exists the steady-state limit with respect to the particle velocities since U_t vanishes in time; however, the decrease rate does not result in the limit for the displacement which grows unboundedly. Nevertheless, the limit exists in term of relative displacement between different points in a finite region. Note that this is associated with the 2D infinite domain; the displacement has a finite limit in the 3D case.

Thus, the steady-state formulation is acceptable for the determination of the particle velocities and the disturbed shape of the half-plane boundary. The asymptotic representation of the vertical displacement at the center of the load support, $x=vt$, which is valid for nonzero subsonic speeds, except the Rayleigh wave speed, follows from (18) as

$$u(vt,t) = \int_0^{x/v} G_\varepsilon(x,t)\,\mathrm{d}t \sim -\frac{Q_y v^2}{\pi\mu c_2^2}\left(u_\infty + \Re\frac{\sqrt{1-v^2/c_1^2-\mathrm{i}0}}{R(v+\mathrm{i}0)}\ln\frac{vt}{\varepsilon}\right) \quad (x = vt,\ vt/\varepsilon\to\infty),$$

$$u_\infty = \Re\int_0^1 \frac{f(\tau)-f(1)}{1-\tau}\mathrm{d}\tau, \quad f(\tau) = \frac{\sqrt{1-v^2/(c_1^2\tau^2)-\mathrm{i}0}}{\tau^3 R(v/\tau+\mathrm{i}0)}. \tag{26}$$

In this asymptotic representation, we take into account the constant term along with the logarithmic one because the latter increases very slowly.

It can be seen in (26) that the logarithmic term does not exist for $v = \sqrt{2}c_2$ and for the supersonic regime (in these cases, the coefficient of the logarithm is pure imaginary). Thus, at these speeds the displacement have the steady-state limit as well as its derivative.

For the Rayleigh wave speed

$$G_\varepsilon \sim -\frac{Q_y c_R^3\sqrt{1-c_R^2/c_1^2}}{\pi\mu c_2^2(c_R-v)R'(c_R)}\frac{\eta}{\eta^2+\varepsilon^2} \quad (x = c_Rt+\eta,\ v\neq c_R,\ 0<v<c_2),$$

$$G_\varepsilon \sim -\frac{Q_y c_R^3\sqrt{1-c_R^2/c_1^2}}{\pi\mu c_2^2 R'(c_R)}\frac{(\eta^2-\varepsilon^2)t}{(\eta^2+\varepsilon^2)^2} \quad (x = c_Rt+\eta,\ v = c_R) \tag{27}$$

the steady-state regime at the Rayleigh wave speed, $v = c_R$, cannot be reached.

For $v = c_1$

$$G_\varepsilon \sim \frac{Q_y c_1^3 c_2^2}{\pi\mu(c_1^2-2c_2^2)^2\sqrt{c_1 t}}\frac{\sqrt{\sqrt{\eta^2+\varepsilon^2}-\eta}}{\sqrt{\eta^2+\varepsilon^2}}. \tag{28}$$

It follows that the particle velocities and the displacements in the vicinity of $x = c_1t$ tend to zero. It is remarkable that this statement is entirely valid for a distributed load ($\varepsilon > 0$), but not for the concentrated one ($\varepsilon = 0$). Indeed, at the limit, $\varepsilon = 0$, the square-root type singular point arises as const $\times H(-\eta)/\sqrt{-t\eta}$, which, however, vanishes by its intensity as $t\to\infty$. At this speed, the true Green's function for the displacements ($\varepsilon = +0$) can be found from (18) as

$$u_y(x) = \frac{Q_y c_1^2 H(c_1^2t^2-x^2)}{\pi\mu c_2^2}\int_{x/(c_1t)}^1 \sqrt{\frac{1+\xi}{1-\xi}}\,\Re\left[\frac{1}{R(c_1\xi)}\right]\xi^2\,\mathrm{d}\xi. \tag{29}$$

The corresponding plot, $U(X) = u_y(X)\pi\mu/Q$ with $X = x/(c_1t)$, is presented in Fig. 2. As shown below, Section 3, Fig. 6, the steady-state regime for a smooth indenter, moving at this speed, corresponds to zero driving force.

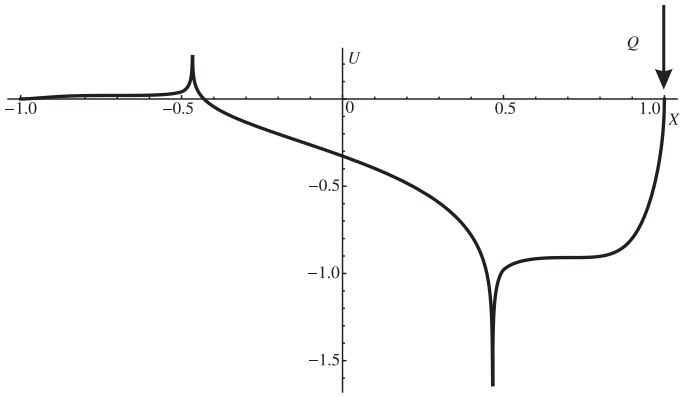

Fig. 2. The normalized displacement caused by a concentrated normal force moving at the longitudinal wave speed ($v=c_1$), $U(X)=u_y(X)\pi\mu/Q$ with $X=x/(c_1t)$. The transient problem.

2.3. The steady-state limit for a general load

In the following, considering the steady-state regime, we express the solution in the moving coordinates. With this in mind in the following we keep notation x instead of η as x belongs to the moving coordinate system, the origin of which is attached to the lower point of the boundary of the moving body as indicated in Figs. 1, 7 and 11. Recall that in these terms, $\partial/\partial t=-v\partial/\partial x$.

Consider the relation between the load (7) and the steady-state limit of $u_y'(x)$ (20). It can be seen that both quantities are expressed in terms of one analytical function as follows:

$$\sigma_{yy}(x)=-Q_y\Im\frac{1}{\pi\zeta},\quad u_y'(x)=\frac{Q_y}{\mu}\Re\frac{1}{\pi\Omega(v)\zeta},$$
$$\Omega(v)=\frac{c_2^2R(v+\mathrm{i}0)}{v^2\sqrt{1-v^2/c_1^2-\mathrm{i}0}},\quad \zeta=x+\mathrm{i}\varepsilon. \tag{30}$$

In the limit, $\varepsilon\to+0$, the stress corresponds to the Dirac delta function (multiplied by Q_y); hence the expression for $u_y'(x)$ becomes the corresponding Green's function. So we write

$$u_y'(x)=\lim_{\varepsilon\to+0}\Re\frac{1}{\pi\Omega(v)\zeta}\quad\text{corresponds to}\quad\sigma_{yy}(x)=-\mu\lim_{\varepsilon\to+0}\Im[1/(\pi\zeta)]=\mu\delta(x). \tag{31}$$

Let an arbitrarily given stress distribution be $\sigma_0(x)$. We make a convolution on x of $\sigma_0(x)$ with each part of the relation in (31), or, which is the same, the convolution with the pre-delta. We find that if

$$\phi(\zeta)=-\frac{1}{\mu\pi}\int_{-\infty}^{\infty}\frac{\sigma_0(\xi)}{\xi-\zeta}\mathrm{d}\xi\quad(\varepsilon>0) \tag{32}$$

then

$$\sigma_{yy}(x)=-\mu\lim_{\varepsilon\to+0}\Im\phi(\zeta),\quad u_y'(x)=\lim_{\varepsilon\to+0}\Re\frac{\phi(\zeta)}{\Omega(v)}. \tag{33}$$

We define

$$\Omega(v)=\frac{c_2^2R(v)}{v^2\alpha_1(v)}=\omega_1(v)+\mathrm{i}\omega_2(v),\quad\frac{1}{\Omega(v)}=\psi_1(v)+\mathrm{i}\psi_2(v), \tag{34}$$

where $\omega_{1,2}(v)$,$\psi_{1,2}(v)$ are real.

In these terms

$$u_y'(x)=-\frac{\psi_1(v)}{\mu\pi}V.p.\int_{-\infty}^{\infty}\frac{\sigma_0(\xi)}{\xi-x}\mathrm{d}\xi+\frac{\psi_2(v)}{\mu}\sigma_{yy}(x). \tag{35}$$

Replacing in (33) $\phi(\zeta)\to\phi(\zeta)\Omega(v)$ we obtain the inverse relation

$$\sigma_{yy}(x)=-\mu\lim_{\varepsilon\to+0}\Im[\Omega(v)\phi(\zeta)]=\mu\left[\frac{\omega_1(v)}{\pi}V.p.\int_{-\infty}^{\infty}\frac{u_y'(\xi)}{\xi-x}\mathrm{d}\xi-\omega_2u_y'(x)\right],$$
$$u_y'(x)=\lim_{\varepsilon\to+0}\Re\phi(\zeta), \tag{36}$$

with

$$\phi(\zeta)=\frac{1}{\pi\mathrm{i}}\int_{-\infty}^{\infty}\frac{u_y'(\xi)}{\xi-\zeta}\mathrm{d}\xi\quad(\varepsilon>0). \tag{37}$$

These relations, where $\sigma_{yy}(x)$ and $u_y'(x)$ are expressed through one analytical function, represent the base for the solution of the mixed problems considered below. Note that a homogeneous solution can be added, which must satisfy conditions at infinity and other conditions of the problem, as done, for example, in (42).

3. The half-plane steady-state contact problem

We consider the steady-state regime of frictionless-contact of a smooth rigid body moving along a half-plane boundary. The plane strain dynamic problem is examined with conditions at the boundary, $y=0$

$$u'(x)=y'(x),\ x\in(x_-,x_+);\quad \sigma_{yy}=0,\ x\notin(x_-,x_+);$$
$$u'(x)=O(1/|x|)\quad |x|\to\infty. \tag{38}$$

Recall that a moving coordinate system is used.

The solution is obtained for any speed and for an arbitrary shape of the indenter such that it corresponds to a single simply connected contact domain. For the parabolic indenter the distributions of the contact stresses and the displacements are presented explicitly. Then each speed range is examined in more detail. Although the solutions to this problem for the sub-Rayleigh and supersonic speed regimes and for the special intersonic speed $v=\sqrt{2}c_2$ are known, for completeness we present the corresponding simplest results among the others.

3.1. General speed solution

Referring to relations (36)–(37) and (11) we introduce a new analytical function of the complex variable $\zeta=x+i\varepsilon$, $\varepsilon>0$

$$\Phi(\zeta)=\Psi(\zeta)\phi(\zeta),\quad \Psi(\zeta)=(\zeta-x_-)^{1/2+\nu}(x_+-\zeta)^{1/2-\nu},$$
$$0\le\nu=\frac{1}{\pi}\arctan\frac{\omega_2(\nu)}{\omega_1(\nu)}\le\frac{1}{2}, \tag{39}$$

with[1]

$$\Psi(x)=(x-x_-)^{1/2+\nu}(x_+-x)^{1/2-\nu}\quad (x_-<x<x_+),$$
$$=-i(x-x_-)^{1/2+\nu}(x-x_+)^{1/2-\nu}e^{i\pi\nu}\quad (x>x_+),$$
$$=i(x_--x)^{1/2+\nu}(x_+-x)^{1/2-\nu}e^{i\pi\nu}\quad (x<x_-). \tag{40}$$

The real part of this function is known on the whole x-axis

$$\Re\Phi(x)=\Psi(x)y'(x)\ \ (x_-<x<x_+),\quad \Re\Phi(x)=0\ \ (x<x_-,x>x_+), \tag{41}$$

where $y(x)$ is the coordinate of the indenter lower surface. We define this function by means of the Cauchy type integral with an additional imaginary constant

$$\Phi(\zeta)=\frac{1}{\pi i}\int_{x_-}^{x_+}\frac{\Psi(\xi)y'(\xi)}{\xi-\zeta}d\xi+iC. \tag{42}$$

It follows from (42) and (36) that the contact stresses[2] are

$$\sigma_{yy}(x)=\mu\left[\frac{\omega_1(\nu)}{\Psi(x)}\left(\frac{1}{\pi}V\cdot p\cdot\int_{x_-}^{x_+}\frac{\Psi(\xi)y'(\xi)}{\xi-x}-C\right)-\omega_2(\nu)y'(x)\right]. \tag{43}$$

Quantities $\omega_{1,2}$ and ν as functions of the speed, v, are plotted in Fig. 3.

Outside the contact region

$$u_y'(x)=-\frac{\cos\pi\nu}{(x-x_+)^{1/2-\nu}(x-x_-)^{1/2+\nu}}\left[\frac{1}{\pi}\int_{x_-}^{x_+}\frac{\Psi(\xi)y'(\xi)}{x-\xi}d\xi+C\right]\quad (x>x_+),$$
$$=\frac{\cos\pi\nu}{(x_+-x)^{1/2-\nu}(x_--x)^{1/2+\nu}}\left[C-\frac{1}{\pi}\int_{x_-}^{x_+}\frac{\Psi(\xi)y'(\xi)}{\xi-x}d\xi\right]\quad (x<x_-). \tag{44}$$

Then we have to eliminate the singularity at $x=x_-$. For $\nu>0$ it is too strong and it cannot be accepted because it corresponds to an infinite energy. For $\nu=0$ it leads to violation of condition (b) in (1) (if $v<c_R$) or condition (c) in (1) (for $c_R<v\le c_2$). Note that this requirement is also in agreement with the finite-stress condition introduced in Barenblatt and Cherepanov (1960) for the leading separation point (in the case of a smooth semi-infinite wedge—for sub-Rayleigh speeds) and in Barenblatt and Goldstein (1972) for the rear end point (in the case of a smooth wedge adjacent to the crack tip—for super-Rayleigh subsonic speeds). However, this condition cannot be applied to the leading separation point for an indenter moving with the super-Rayleigh speed at a distance from the crack tip.

[1] Note that ν is not Poisson's ratio!

[2] In the following part of this section, for brevity, we will not indicate the contact region, $x\in(x_-,x_+)$, for the contact stresses.

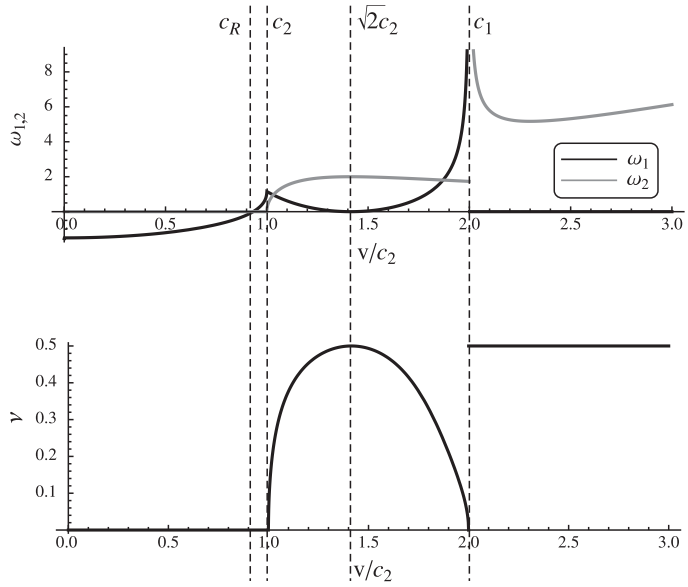

Fig. 3. The real and imaginary parts of the function $\Omega(v)$ (34) and the parameter ν (39), computed for Poisson's ratio equal to 1/3 ($c_1 = 2c_2$).

So we define constant C as

$$C = \frac{1}{\pi}\int_{x_-}^{x_+} \left(\frac{x_+ - \xi}{\xi - x_-}\right)^{1/2-\nu} y'(\xi)\,\mathrm{d}\xi. \tag{45}$$

It is now found that

$$\sigma_{yy}(x) = \mu\left[\left(\frac{x-x_-}{x_+-x}\right)^{1/2-\nu}\frac{\omega_1(\nu)}{\pi}V\cdot p\cdot\int_{x_-}^{x_+}\left(\frac{x_+-\xi}{\xi-x_-}\right)^{1/2-\nu}\frac{y'(\xi)}{\xi-x}\mathrm{d}\xi - \omega_2(\nu)y'(x)\right],$$

$$u_y'(x) = -\left(\frac{x-x_-}{x-x_+}\right)^{1/2-\nu}\frac{\cos\pi\nu}{\pi}\int_{x_-}^{x_+}\left(\frac{x_+-\xi}{\xi-x_-}\right)^{1/2-\nu}\frac{y'(\xi)}{x-\xi}\mathrm{d}\xi \quad (x > x_+),$$

$$u_y'(x) = \left(\frac{x_- - x}{x_+-x}\right)^{1/2-\nu}\frac{\cos\pi\nu}{\pi}\int_{x_-}^{x_+}\left(\frac{x_+-\xi}{\xi-x_-}\right)^{1/2-\nu}\frac{y'(\xi)}{\xi-x}\mathrm{d}\xi \quad (x < x_-). \tag{46}$$

The asymptotic representation for the contact zone ends are

$$u_y'(x) \sim -\left(\frac{x_+-x_-}{x-x_+}\right)^{1/2-\nu}\frac{\cos\pi\nu}{\pi}\int_{x_-}^{x_+}\frac{y'(\xi)\,\mathrm{d}\xi}{(\xi-x_-)^{1/2-\nu}(x_+-\xi)^{1/2+\nu}},$$

$$\sigma_{yy} \sim -\mu\left[\left(\frac{x_+-x_-}{x_+-x}\right)^{1/2-\nu}\frac{\omega_1(\nu)}{\pi}\int_{x_-}^{x_+}\frac{y'(\xi)\,\mathrm{d}\xi}{(\xi-x_-)^{1/2-\nu}(x_+-\xi)^{1/2+\nu}} + \omega_2(\nu)y'(x_+)\right] \tag{47}$$

for $x \to x_+ \pm 0$, respectively, and

$$u_y'(x) \to y'(x_-)\ \ (x \to x_- - 0),\ \ \sigma_{yy} \to 0\ (x \to x_- + 0). \tag{48}$$

These results are valid for any ν, $0 \le \nu \le 1/2$, that is, for any speed regime, $v > 0$.

In the case of symmetric indenter, $y(-x) = y(x)$, and symmetric contact zone, $x_- = -x_+$, (corresponding to the sub-Rayleigh speed regime, where $v = 0$, $\omega_1(v) = \Omega(v) < 0$, $\omega_2(v) = 0$, see Fig. 3) the results can be simplified. Symmetrization leads to

$$\sigma_{yy}(x) = \mu\Omega(v)\sqrt{x_+^2 - x^2}\,\frac{2}{\pi}V\cdot p\cdot\int_0^{x_+}\frac{\xi y'(\xi)}{\sqrt{x_+^2-\xi^2}(\xi^2-x^2)}\mathrm{d}\xi,$$

$$u_y'(x) = \sqrt{x^2 - x_+^2}\,\frac{2}{\pi}\int_0^{x_+}\frac{\xi y'(\xi)}{\sqrt{x_+^2-\xi^2}(x^2-\xi^2)}\mathrm{d}\xi\ \mathrm{sign}\,x \quad (|x| > x_+). \tag{49}$$

For a symmetric parabolic indenter, $u_y'(x) = x/r$, results in (49) specialize to

$$\sigma_{yy}(x) = \frac{\mu\Omega(v)}{r}\sqrt{x_+^2 - x^2},$$

$$u_y'(x) = \frac{1}{r}\left[x - \mathrm{sign}\,x\sqrt{x^2 - x_+^2}\right] \quad (|x| \ge x_+). \tag{50}$$

The displacement profile has the form

$$u(x)=\frac{1}{2r}\left[x^2-|x|\sqrt{x^2-x_+^2}+x_+^2\,\ln\left(|x/x_+|+\sqrt{(x/x_+)^2-1}\right)\right]\quad(|x|\ge x_+),\quad u(x)=\frac{x^2}{2r}\quad(|x|\le x_+).\tag{51}$$

The indenter–half-plain configuration is shown in Fig. 1a left.

For *greater speeds*, $v>c_R$, when $\omega_1\ge 0$, for a parabolic indenter, $u_y'(x)=x/r$, it follows from (46) that

$$\begin{aligned}
&\frac{\sigma_{yy}(x)}{\mu}=-\frac{\omega_1(v)}{\cos\pi v}\left(\frac{x-x_-}{x_+-x}\right)^{1/2-v}\frac{x-x_-+\gamma}{r},\\
&u_y'(x)=\frac{x}{r}+\left(\frac{x_--x}{x_+-x}\right)^{1/2-v}\frac{x_--x-\gamma}{r}\quad(x\le x_-),\\
&u_y'(x)=\frac{x}{r}-\left(\frac{x-x_-}{x-x_+}\right)^{1/2-v}\frac{x-x_-+\gamma}{r}\quad(x>x_+),\\
&\gamma=(1/2-v)x_+-(3/2-v)x_-.
\end{aligned}\tag{52}$$

Note that, in the derivation of these expressions, we have used the identity

$$\int_0^1\left(\frac{1-\xi}{\xi}\right)^{1/2-v}\frac{\mathrm{d}\xi}{\xi-\mathrm{i}\varepsilon}=\frac{\pi}{\cos\pi v}\left[\left(1+\frac{\mathrm{i}}{\varepsilon}\right)^{1/2-v}-1\right]\quad(\Re\varepsilon>0,\ 0\le v<1/2),\tag{53}$$

with the corresponding analytical continuation.

We find from the expression for $\sigma_{yy}(x)$ in (52) that the condition (a) in (1) is satisfied only if $\gamma\ge 0$. On the other hand, as can be seen in the expression for $u_y'(x)$ $(x\le x_-)$ the condition (b) in (1) is satisfied only if $\gamma\le 0$. Thus, to satisfy both conditions the only possibility remains that $\gamma=0$. Now the expressions in (52) [also see (46)] can be rewritten in the form

$$\begin{aligned}
&\sigma_{yy}(x)=-\frac{\mu}{r}\frac{\omega_1(v)}{\cos\pi v}\frac{(x-x_-)^{3/2-v}}{(x_+-x)^{1/2-v}}\quad(\omega_1\ne 0),\\
&\sigma_{yy}(x)=-\mu\omega_2(v)\frac{x}{r}\quad(\omega_1=0,\ \omega_2\ne 0),\\
&u_y'(x)=\frac{x}{r}+\frac{(x_--x)^{3/2-v}}{r(x_+-x)^{1/2-v}}\quad(x\le x_-),\\
&u_y'(x)=\frac{x}{r}-\frac{(x-x_-)^{3/2-v}}{r(x-x_+)^{1/2-v}}\quad(x>x_+),\\
&x_-=\frac{1-2v}{3-2v}x_+.
\end{aligned}\tag{54}$$

Note that the latter relation also results in elimination of the constant terms in the asymptotic representation of $u_y'(x)$ for $x\to\mp\infty$, respectively. For $v<1/2$ they become of order $1/|x|$, for $v=1/2$ the derivatives outside the contact region are zero ($x_-=0$). The plots of x_-/x_+ and of the stress distributions are presented in Figs. 4 and 5, respectively.

3.2. Subsonic regime

In subsonic regime, function $\Omega(v)$ is real, $\Omega(v)<0$ in the sub-Rayleigh speed regime, $0<v<c_R$, and $\Omega(v)>0$ in the super-Rayleigh subsonic speed regime, $c_R<v<c_2$.

Sub-Rayleigh regime. In the sub-Rayleigh speed regime, the stress and displacement derivative distributions are presented in (50). The remaining parameter, that is, the contact zone half-length follows from the equilibrium relation as

$$Q_y=2\int_0^{x_+}\sigma_{yy}(x)\,\mathrm{d}x=\frac{\pi\mu x_+^2\,\Omega(v)}{2r}\Rightarrow x_+=\sqrt{\frac{2rQ_y}{\pi\mu\Omega(v)}}.\tag{55}$$

(Note that $Q_y<0$ and $R(v)$ is also negative in this speed regime.) There is no resistance to the movement.

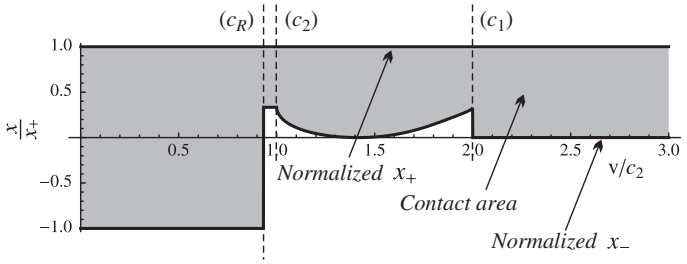

Fig. 4. The normalized contact zone, $x_-/x_+<x/x_+<1$, as a function of the speed, v. Results correspond to Poisson's ratio equal to 1/3 ($c_1=2c_2$). Note that the value of x_+ depends on both v and Q_y (55), (60), (74) and (81). In the case $v=c_1$, $x_+=x_-=0$.

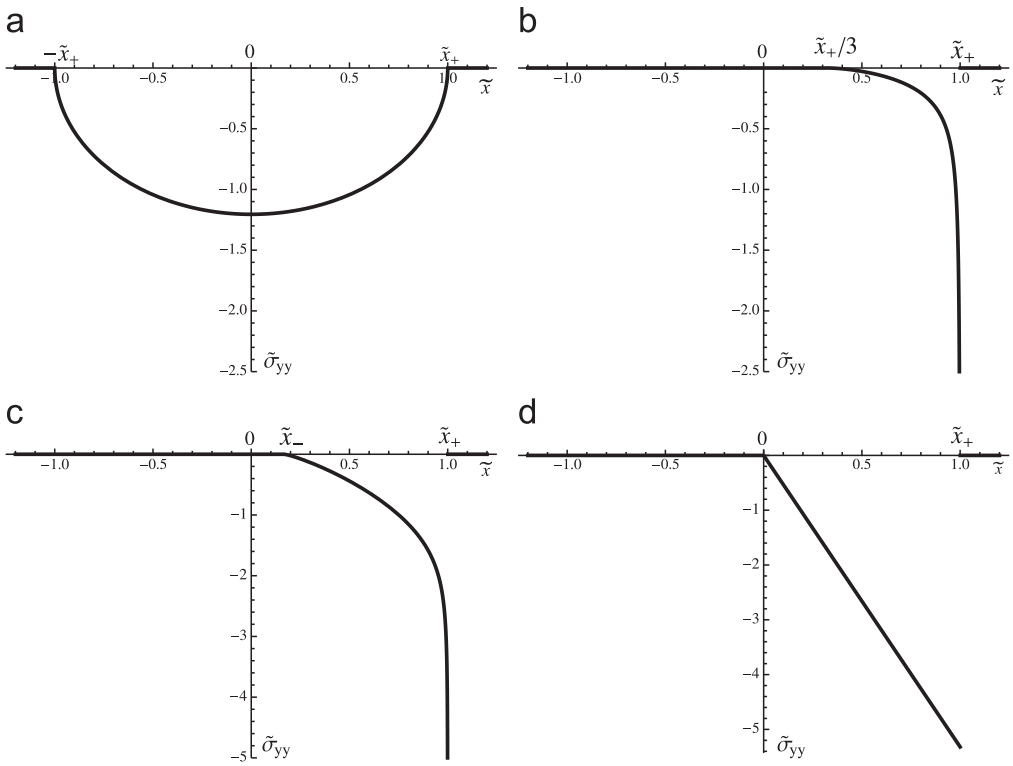

Fig. 5. The contact stress distributions as a function of the normalized coordinate $\tilde{x}=x/x_+$. The plots are based on (50) for sub-Rayleigh speed regime, (54) for super-Rayleigh subsonic and intersonic speed regimes and (81) for the supersonic speed regime. The special case $v=\sqrt{2}c_2$ (77) is the same as in the supersonic regime. At $v=c_1$ the contact zone is localized, $\sigma_{yy}=Q_y\delta(x)$ (83). In the super-Rayleigh subsonic (b) and in the intersonic (c) speed regimes, the leading end points of the contact zone, x_+, are singular, $\sigma_{yy}\to-\infty$ as $x\to x_+-0$. In (b) it is an energy absorbing square-root type point, whereas in (c) it is a weak point, which can neither absorb nor release energy. (a) Sub-Rayleigh regime: $v<c_R$. (b) Super-Rayleigh regime: $c_R<v\le c_2$. (c) Intersonic regime: $c_2\le v<c_1$. (d) Supersonic regime: $v>c_1$.

3.2.1. Zero driving force in the sub-Rayleigh speed regime. a general statement

In the sub-Rayleigh speed regime, $0<v<c_R$, there is no resistance to the movement of a smooth indenter of any shape. Although this statement follows directly from energy considerations, here we present a formal proof. We first note that, in this speed range, in accordance with condition (b) in (1), the remaining singularity at $x=x_+$ must be eliminated. Referring to (46) with $x\to x_+$ we thus have to impose

$$\int_{x_-}^{x_+}\frac{y'(\xi)\,\mathrm{d}\xi}{\sqrt{(x_+-\xi)(\xi-x_-)}}=0. \tag{56}$$

It also follows from (46) that the driving force is

$$P=-\int_{x_-}^{x_+}\sigma_{yy}(x)y'(x)\,\mathrm{d}x=-\frac{\mu\Omega(v)}{\pi}\int_{x_-}^{x_+}\sqrt{\frac{x-x_-}{x_+-x}}P\cdot v\cdot\int_{x_-}^{x_+}\sqrt{\frac{x_+-\xi}{\xi-x_-}}\frac{y'(\xi)y'(x)}{\xi-x}\,\mathrm{d}\xi\,\mathrm{d}x. \tag{57}$$

Consider a sum of the integrant corresponding to points which are symmetric relatively to the singular line, $\xi=x$, that is, points (x,ξ) and (ξ,x). It is

$$\frac{y'(\xi)y'(x)}{\xi-x}\left[\sqrt{\frac{(x-x_-)(x_+-\xi)}{(x_+-x)(\xi-x_-)}}-\sqrt{\frac{(\xi-x_-)(x_+-x)}{(x_+-\xi)(x-x_-)}}\right]=-\frac{y'(\xi)y'(x)(x_+-x_-)}{\sqrt{(x_+-\xi)(\xi-x_-)(x-x_-)(x_+-x)}}. \tag{58}$$

The latter expression is symmetric relatively this line, and we can preserve the integration over the initial square domain, $x_-<(x,\xi)<x_+$. Now we find from (58) and (56) that $P=0$, as it should be.

Note that if the expression in (56) is not equal to zero, that is, if the singularity at $x=x_+$ is not canceled out, the result in (58), with reference to (46), evidences that P is equal to the energy release rate associated with the singular point, thus confirming the validity of the result.

Super-Rayleigh regime. In the super-Rayleigh subsonic regime, $c_R<v<c_2$, where $\Omega(v)>0$, the contact zone is defined in (54) with $v=0$

$$x_-=\frac{x_+}{3}. \tag{59}$$

The stress and displacement's derivative distributions are also presented in (54). This solution corresponds to the vertical force

$$Q_y = \int_{x_+/3}^{x_+} \sigma_{yy}\, \mathrm{d}x = -\frac{\pi\Omega(v)\mu x_+^2}{6r} \tag{60}$$

applied at position

$$x = x_Q = \int_{x_+/3}^{x_+} x\sigma_{yy}\mathrm{d}x \Big/ \int_{x_+/3}^{x_+} \sigma_{yy}\, \mathrm{d}x = \frac{8}{9}x_+ . \tag{61}$$

In this case, the front end point of the contact zone, x_+, is the singular point of the square root type, and there exists the energy flux to this point. The corresponding stress intensity factor is

$$K_I \equiv \lim_{x\to x_+-0} \sigma_{yy}\sqrt{2\pi(x_+ - x)} = -\left(\frac{2x_+}{3}\right)^{3/2} \frac{\sqrt{2\pi}\mu\Omega(v)}{r} \tag{62}$$

and the energy release rate is

$$G = \frac{K_I^2}{4\mu\Omega(v)} = \frac{4\pi\mu\Omega(v)x_+^3}{27r^2} = \frac{8}{9}Q\sqrt{\frac{6Q}{\pi\Omega(v)\mu r}}. \tag{63}$$

(The relation between the energy release rate and the stress intensity factors for crack dynamics was introduced in Kostrov et al., 1969.) This relation (see Fig. 6) just corresponds to the horizontal driving force

$$P = -\int_{x_+/3}^{x_+} \sigma_{yy}(x)u_y'(x)\mathrm{d}x = G, \tag{64}$$

which is not surprising since there is no wave radiation at these speeds, and the energy produced by the contact stresses completely goes to the singular point. Recall that this driving force can be equally treated as a Newtonian horizontal force or as a configurational force. The nondimensional $P-Q$ relation looks as

$$\mathcal{P} = \frac{P}{Q}\sqrt{\frac{\mu r}{Q}} = \frac{8}{9}\sqrt{\frac{6}{\pi\Omega(v)}}. \tag{65}$$

The equality $P=G$ confirms that no wave is radiated in this speed regime. In this connection, note that the radiation mentioned in Barenblatt and Goldstein (1972) can be caused by an energy-source singular point existing at the crack tip in the super-Rayleigh speed regime.

The displacement profile has the form

$$\begin{aligned}
u(x) &= \frac{x_+^2}{2r}\left\{\tilde{x}^2 + (\tilde{x}+2/3)\sqrt{(1-\tilde{x})(1/3-\tilde{x})} + \frac{2}{3}\ln\left[\sqrt{3/2}\left(\sqrt{1-\tilde{x}} + \sqrt{1/3-\tilde{x}}\right)\right]\right\} \quad (x \le x_+/3),\\
u(x) &= \frac{x^2}{2r} \quad (x_+/3 \le x \le x_+),\\
u(x) &= \frac{x_+^2}{2r}\left\{\tilde{x}^2 - (\tilde{x}+2/3)\sqrt{(\tilde{x}-1)(\tilde{x}-1/3)} - \frac{2}{3}\ln\left[\sqrt{3/2}\left(\sqrt{\tilde{x}-1} + \sqrt{\tilde{x}-1/3}\right)\right]\right\} \quad (x \ge x_+),
\end{aligned} \tag{66}$$

where $\tilde{x} = x/x_+$. The indenter–half-plain configurations are shown in Fig. 1a right.

What happens at the front singular points, through which the energy releases under compression? What happens to this energy, where is it spent? The classical elasticity cannot answer these questions, whereas a 'micro'-structure mechanisms of energy dissipation can be different. One of them is plasticity. Indeed, in the vicinity of the singular point,

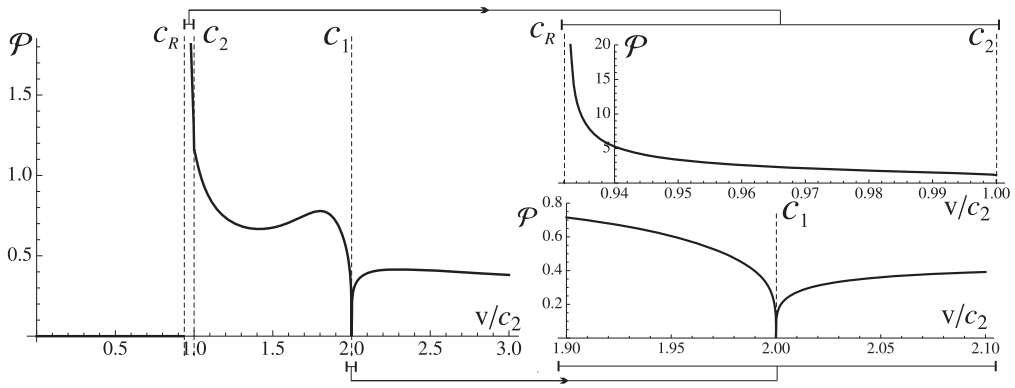

Fig. 6. The driving force–vertical force relation: $\mathcal{P} = P/[Q\sqrt{\mu r/Q}]$ as a function of the speed, v. It can be seen that the resistance to the movement is zero at sub-Rayleigh speeds. It drops down sharply in the vicinity of the longitudinal wave speed, c_1 ($v \to c_1 \pm 0$).

the normal stresses are (see, e.g., Slepyan, 2002, pp. 303–304)

$$\sigma_{xx}(x)\sim-\sigma_{yy}\left[1+\frac{2(\alpha_1^2(v)-\alpha_2^2(v))(1+\alpha_2^2(v))}{R(v)}\right],\quad \sigma_{yy}(x)\sim\frac{K_I}{\sqrt{2\pi(x_+-x)}}. \tag{67}$$

In this case, $\sigma_{yy}(x)<0$ ($K_I<0$), $\sigma_{xx}(x)>0$ and $\sigma_{xx}(x)>|\sigma_{yy}(x)|$. Thus this point is singular with respect to shear stresses. This suggests that plastic deformations, possibly with melting, can occur in a surface layer. For a brittle material, high level tensile stresses can result in cracking and fragmentation of the surface layer. Note that latter inequality was mentioned in Barenblatt and Cherepanov (1960) for the case of a moving wedge approaching the Rayleigh wave speed from below.

3.2.2. The crack healing limit

Expressions (54), which is valid for the parabolic indenter, can be reduced to match the super-Rayleigh subsonic speed regime of crack closure. For this regime, where $v=0$, $\omega_1(v)=\Omega(v)>0$, we put

$$r\to\infty,\quad x_+\to\infty,\quad \frac{((2/3)x_+)^{3/2}}{r}\to\sqrt{a}\quad (a>0),$$
$$u_y(x_+)=0,\quad x\to x_++x. \tag{68}$$

For any finite x we find

$$u_y(x)=0\quad (x\le 0),\quad u_y(x)=-\sqrt{2ax}\ (x\ge 0),$$
$$\sigma_{yy}(x)=-\mu\Omega(v)\sqrt{a/(-x)}H(-x)\quad (c_R<v\le c_2), \tag{69}$$

where the displacement corresponds to the lower half-plane. The equilibrium is achieved by adding a symmetrically disturbed upper half-plane. As a result we have the super-Rayleigh subsonic speed regime of the crack closure with the energy absorbing singular point, $x=0$ (recall that x is the moving coordinate), the end point of the semi-infinite crack, $0<x<\infty$. Now the energy is coming from infinity; the energy release rate is

$$G=\pi\mu a\Omega(v). \tag{70}$$

If G is large enough the crack healing may be expected. The limit, a, depends on the speed. Assume the healing criterion to be $G=G_c=\text{const}$; it follows that the critical value of the above limit and the critical stress intensity factor are

$$a=a_c(v)=\frac{G_c}{\pi\mu\Omega(v)},\quad K_{Ic}(v)=-\sqrt{2\mu G_c\Omega(v)}. \tag{71}$$

The latter relation is in agreement with the Kostrov–Nikitin–Flitman formula (Kostrov et al., 1969). Thus the critical stress intensity factor increases by its modulus from zero to

$$K_{max}=K_{Ic}(c_2)=-\sqrt{\frac{2\mu G_c}{\sqrt{1-c_2^2/c_1^2}}} \tag{72}$$

as the speed growth from c_R to c_2.

Note that this crack related solution follows, of course, directly from the corresponding problem formulation. We here have shown only the connection with the contact problem.

3.3. Intersonic regime

The general relations for this regime and those for a parabolic indenter are presented in Section 3.1. In the transition from the subsonic speed range to the intersonic one, the solution varies continuously. Parameter v grows from zero to 1/2 as the speed increases from c_2 to $\sqrt{2}c_2$; then it decreases to zero as $v\to c_1$. Thus $0<v\le 1/2$ for $c_2<v<c_1$. Under these inequalities the strongest singular point at $x=x_+$ is weak in the sense that it cannot conduct energy. However, in this speed range, shear waves arise excited by the moving body. Thus, in the intersonic range, a driving force is required to support the movement. It is

$$P=\frac{4\pi\mu(1-v)(1-2v)\omega_1(v)x_+^3}{3(3-2v)^2\cos^2(\pi v)r^2}, \tag{73}$$

whereas the vertical force is

$$Q_y=-\frac{\pi\mu(1-2v)\omega_1(v)x_+^2}{2(3-2v)\cos^2(\pi v)r}. \tag{74}$$

The indenter–half-plane configuration is shown in Fig. 1b. The nondimensional ratio

$$\mathcal{P}=\frac{P}{Q}\sqrt{\frac{\mu r}{Q}}=\frac{16(1-v)\cos\pi v}{3\sqrt{2\pi(1-2v)(3-2v)\omega_1(v)}} \tag{75}$$

as a function of v is plotted in Fig. 6 for Poisson's ratio equal 1/3 ($c_1=2c_2$). For the super-Rayleigh subsonic range the plot is based on (65).

3.4. Special speed value, $v=\sqrt{2}c_2$, and the supersonic regime

At this *intersonic speed* $v=1/2$, $\omega_1=0$, $\omega_2=2$, $x_-=0$, and, as it follows directly from (43),

$$\sigma_{yy}(x)=-2\mu u_y'(x),\quad Q_y=-2\mu y(x_+). \tag{76}$$

For the parabolic indenter the contact stresses, the vertical force and the driving force are

$$\sigma_{yy}(x)=-\frac{2\mu x}{r},\quad Q_y=-\frac{\mu x_+^2}{r},\quad P=\frac{2\mu x_+^3}{3r^2}, \tag{77}$$

respectively, which is also in agreement with the limit ($v\to 1/2$) following from (73) and (74). The half-plane boundary outside the contact zone is horizontal, whereas there is a shift in the displacement

$$u_y'(x)=0\ \ (x<0,\ x>x_+),\quad u_y(x_+)-u_y(0)=y(x_+). \tag{78}$$

The solution of the same type corresponds to the *supersonic regime*, which differs by the presence of both the shear and the longitudinal waves. In the transition to this regime, parameter v has a jump discontinuity from zero at $v=c_1-0$ to $1/2$ at $v>c_1$ (see Fig. 3). For the latter regime

$$\omega_1(v)=0,\quad \omega_2(v)=\frac{c_2^2R(v)}{v^2\sqrt{v^2/c_1^2-1}}, \tag{79}$$

where the corresponding expression for the Rayleigh function, $R(v)$ is shown in (11). Thus, the stresses and the vertical force are

$$\sigma_{yy}(x)=-\mu\omega_2(v)u_y'(x),\quad Q_y=-\frac{\mu\omega_2(v)y(x_+)}{r}. \tag{80}$$

For the parabolic indenter the contact stresses, the vertical force and the driving force are

$$\sigma_{yy}(x)=-\frac{\mu\omega_2(v)x}{r},\quad Q_y=-\frac{\mu\omega_2(v)x_+^2}{2r},\quad P=\frac{\mu\omega_2(v)x_+^3}{3r^2},$$
$$\mathcal{P}=\frac{P}{Q}\sqrt{\frac{\mu r}{Q}}=\frac{2}{3}\sqrt{\frac{2}{\omega_2(v)}}. \tag{81}$$

3.5. The limiting resistance-free steady-state regime, $v\to c_1$

It follows from (73) and (81) that, for nonzero Poisson's ratio,

$$\mathcal{P}\sim\frac{16}{3\sqrt{6\pi\omega_1(v)}}\to 0\quad(\omega_1\to\infty \text{ as } v\to c_1-0),$$
$$\mathcal{P}\to 0\quad(\omega_2\to\infty \text{ as } v\to c_1+0). \tag{82}$$

In this case $x_+=x_-=0$, and the indenter, under the external vertical force Q_y, is in equilibrium with a concentrated longitudinal wave propagating in the half-plane. Thus, this is a special case of d'Alembert's paradox manifestation

$$x_+=x_-=0,\quad \sigma_{yy}=Q_y\delta(x),\quad P=0\ \ (v=c_1). \tag{83}$$

Recall that this result corresponds to the limit, $v\to c_1$, of the established steady-state regimes for $v<c_1$ and $v>c_1$.

4. Wedging

The plane problem for the motion of a rigid symmetric wedge through the elastic material is examined in this section. To avoid geometrical nonlinearities we do not consider the case when the wedge is to close to the crack tip. We derive the exact solution for the sub-Rayleigh regime. A simplified solution is also given based on the assumption that the contact zone is much shorter than its distance to the crack tip.

First we note that there is no crack closure in the considered problem. This follows from relation (5.73) in Slepyan (2002), which remains qualitatively valid for the sub-Rayleigh speed regime. It can be seen in this relation that, for compressive crack face traction, the crack opening behind the contact zone ($x<x_-$) remains positive and it tends to zero as $x\to-\infty$. Thus the traction behind the contact region is zero. Denote the contact region end points and the crack tip coordinates as $x_-<x_+<x_c$, respectively (see Fig. 7). The conditions on the lower half-plane boundary (and similar conditions on the upper half-plane boundary) are

$$u_y(x)=y(x)\ \ (x_-<x<x_+),\quad u_y(x)=h\ \ (x\ge x_c),$$
$$u_y'(x)=O(|x|^{-3/2})\ \ (x\to-\infty),\quad \sigma_{yy}=0\ \ (x<x_-\text{ and } x_+<x<x_c), \tag{84}$$

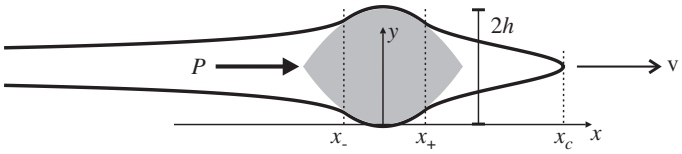

Fig. 7. Crack face contour in the wedging, $v < c_R$.

where h is the wedge half-width (the origin of the coordinates coincides with the lower point of the wedge as above). We use the same representation as above, namely for $v < c_R$,

$$u_y'(x) = \Re\phi(x), \quad \sigma_{yy}(x) = -\mu\Omega(v)\Im\phi(x), \tag{85}$$

where $\phi(\zeta)$ is an analytical function of the complex variable $\zeta = x + i\varepsilon$, $\varepsilon > 0$. Next, another analytical function is introduced as

$$\Phi(\zeta) = \Psi(\zeta)\phi(\zeta), \quad \Psi(\zeta) = \sqrt{(\zeta - x_-)(\zeta - x_+)(\zeta - x_c)}, \tag{86}$$

where

$$\Psi(x) = \begin{cases} \sqrt{(x-x_-)(x-x_+)(x-x_c)} & (x > x_c), \\ i\sqrt{(x-x_-)(x-x_+)(x_c-x)} & (x_+ < x < x_c), \\ -\sqrt{(x-x_-)(x_+-x)(x_c-x)} & (x_- < x < x_+), \\ -i\sqrt{(x_--x)(x_+-x)(x_c-x)} & (x < x_-). \end{cases} \tag{87}$$

Since outside the contact region $\Re\Phi(x) = 0$, we can express this function in the same way as above

$$\Phi(\zeta) = \frac{i}{\pi}\int_{x_-}^{x_+} \frac{y'(\xi)\sqrt{(\xi - x_-)(x_+ - \xi)(x_c - \xi)}}{\xi - \zeta}\,d\xi + iC. \tag{88}$$

Now consider the stress intensity at the end points. It follows from (85) and (88) that

$$\begin{aligned} &\lim_{x\to x_- + 0}\sigma_{yy}(x)\sqrt{x - x_-} = \frac{\mu\Omega(v)}{\sqrt{(x_+ - x_-)(x_c - x_-)}}\left(\frac{1}{\pi}\int_{x_-}^{x_+}\sqrt{\frac{(x_+ - \xi)(x_c - \xi)}{\xi - x_-}}y'(\xi)\,d\xi + C\right), \\ &\lim_{x\to x_+ - 0}\sigma_{yy}(x)\sqrt{x_+ - x} = -\frac{\mu\Omega(v)}{\sqrt{(x_+ - x_-)(x_c - x_+)}}\left(\frac{1}{\pi}\int_{x_-}^{x_+}\sqrt{\frac{(\xi - x_-)(x_c - \xi)}{x_+ - \xi}}y'(\xi)\,d\xi - C\right), \\ &\lim_{x\to x_c + 0}\sigma_{yy}(x)\sqrt{x - x_c} = \frac{\mu\Omega(v)}{\sqrt{(x_c - x_-)(x_c - x_+)}}\left(\frac{1}{\pi}\int_{x_-}^{x_+}\sqrt{\frac{(x_+ - \xi)(\xi - x_-)}{x_c - \xi}}y'(\xi)\,d\xi - C\right). \end{aligned} \tag{89}$$

For the sub-Rayleigh speed regime the stress intensities at the contact region ends, $x = x_\pm$, must be zero to avoid interpenetration. Let the stress intensity factor at the crack tip be given as K_I. These three conditions lead to the following relations:

$$\begin{aligned} &C = -\frac{1}{\pi}\int_{x_-}^{x_+}\sqrt{\frac{(x_+ - \xi)(x_c - \xi)}{\xi - x_-}}y'(\xi)\,d\xi, \\ &\int_{x_-}^{x_+}\sqrt{\frac{x_c - \xi}{(\xi - x_-)(x_+ - \xi)}}y'(\xi)\,d\xi = 0, \\ &\mu\Omega(v)\sqrt{\frac{x_c - x_-}{x_c - x_+}}\frac{1}{\pi}\int_{x_-}^{x_+}\sqrt{\frac{x_+ - \xi}{(\xi - x_-)(x_c - \xi)}}y'(\xi)\,d\xi = \frac{K_I}{\sqrt{2\pi}}. \end{aligned} \tag{90}$$

An additional condition concerning the wedge maximal width 2 h must be taken into account; recalling that the coordinate of the maximal width is taken as the origin of the x-axis the following equation is obtained:

$$y(x_+) + \int_{x_+}^{x_c} u_y'(x)\,dx = h, \tag{91}$$

where, in this region, $x_+ < x < x_c$

$$u_y'(x) = \sqrt{\frac{x - x_-}{(x - x_+)(x_c - x)}}\frac{1}{\pi}\int_{x_-}^{x_+}\sqrt{\frac{(x_+ - \xi)(x_c - \xi)}{\xi - x_-}}\frac{y'(\xi)}{\xi - x}\,d\xi. \tag{92}$$

Finally, the nonzero normal stress component is

$$\sigma_{yy}(x) = \mu\Omega(v)\sqrt{\frac{x - x_-}{(x_+ - x)(x_c - x)}}\frac{1}{\pi}V\cdot p\cdot\int_{x_-}^{x_+}\sqrt{\frac{(x_+ - \xi)(x_c - \xi)}{\xi - x_-}}\frac{y'(\xi)}{\xi - x}\,d\xi \tag{93}$$

in the contact region ($x_- < x < x_+$) and

$$\sigma_{yy}(x) = -\mu\Omega(v)\sqrt{\frac{x-x_-}{(x-x_+)(x-x_c)}}\frac{1}{\pi}\int_{x_-}^{x_+}\sqrt{\frac{(x_+-\xi)(x_c-\xi)}{\xi-x_-}}\frac{y'(\xi)}{\xi-x}\,d\xi \tag{94}$$

ahead of the crack tip.

Thus, three unknowns remain: x_-, x_+ and x_c; they can be obtained from (91) and the last two relations in (90). In particular, it follows from the second relation in (90) that $x_- < 0$ and $x_+ > 0$.

4.1. The parabolic wedge

For the parabolic wedge, $y(x) = x^2/(2r)$, the second condition in (90) and Eq. (91) lead to the following relations:

$$(x_c-x_+)K\left(\frac{x_+-x_-}{x_c-x_-}\right)-(x_c-2x_+-2x_-)E\left(\frac{x_+-x_-}{x_c-x_-}\right)=0, \tag{95}$$

$$\frac{\mu\Omega(v)(x_c-x_-)}{3\pi r}\left[K\left(\frac{x_+-x_-}{x_c-x_-}\right)(2x_c+x_-)-E\left(\frac{x_+-x_-}{x_c-x_-}\right)(2x_c+2x_--x_+)\right]=\frac{K_I}{\sqrt{2\pi}}, \tag{96}$$

where $K(m) = \int_0^{\pi/2}(1-m\sin^2\theta)^{-1/2}\,d\theta$ and $E(m) = \int_0^{\pi/2}(1-m\sin^2\theta)^{1/2}\,d\theta$ are the complete elliptic integrals of the first and second kind, respectively.

To proceed we make some simplification assuming the contact zone to be much shorter than its distance to the crack tip, $x_+ - x_- \ll x_c - x_*$, $x_* = (x_+ + x_-)/2$, namely, for the integrals over the contact region we replace $\sqrt{x_c-\xi}$, where $\xi \in (x_-, x_+)$, by its two-term asymptote as

$$\sqrt{x_c-\xi} \sim \sqrt{x_c-x_*}+\frac{x_*-\xi}{2\sqrt{x_c-x_*}}, \quad \frac{1}{\sqrt{x_c-\xi}} \sim \frac{1}{\sqrt{x_c-\xi}}-\frac{x_*-\xi}{2(x_c-x_*)^{3/2}}. \tag{97}$$

The second condition in (90) of zero stress intensity at x_+ leads now to an explicit expression for x_c in terms of $x_\pm$

$$x_c = \frac{5x_+^2+6x_+x_-+5x_-^2}{8(x_++x_-)}. \tag{98}$$

Note that $x_c \to \infty$ when $x_- \to -x_+ + 0$ as it should be (in the limit, we have a half-plane under the moving indenter, that is, we return the previous problem), and $x_- \to -3/5x_+$ when $x_c \to x_+ + 0$.

The relative position of the crack tip $\tilde{x}_c = x_c/x_+$ as a function of the ratio $\tilde{x}_- = x_-/x_+$ is shown in Fig. 8, where the approximate result (98) is compared with the exact one following from (95). It is evident that the approximation can be acceptable for $\tilde{x}_c > 2$.

Next, the last condition in (90) concerning the stress intensity at x_c yields

$$\frac{\mu\Omega(v)}{2r}\frac{7x_+^2+18x_+x_-+7x_-^2}{\sqrt{(5x_++3x_-)(-3x_+-5x_-)}}\sqrt{x_++x_-}=\frac{K_I}{\sqrt{\pi}}. \tag{99}$$

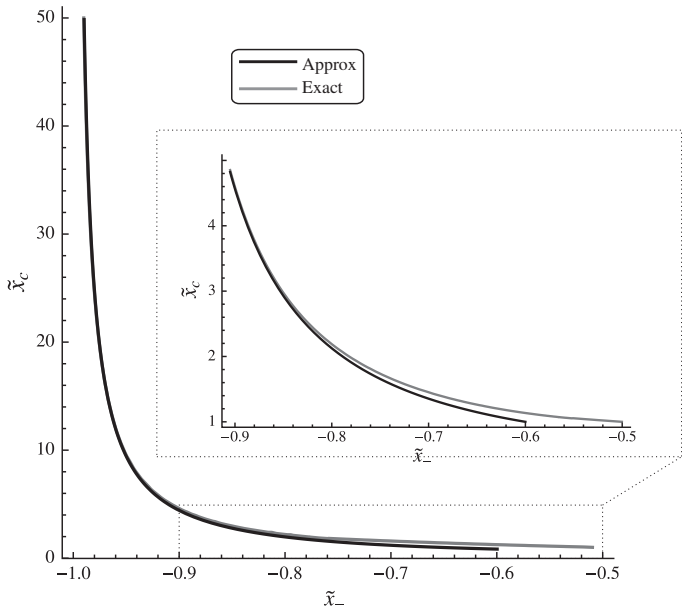

Fig. 8. Distribution of the normalized position of the crack tip, $\tilde{x}_c = x_c/x_+$, as a function of the ratio $\tilde{x}_- = x_-/x_+$ for the parabolic indenter. Approximate results (in black) are compared with the exact one (in gray).

We also represent this relation in a normalized form as

$$\Omega(v)\hat{x}_+^{3/2} g_w(\tilde{x}_-) = M_w, \tag{100}$$

with

$$M_w = 2\left(\frac{r}{h^3}\right)^{1/4} \frac{K_I}{\sqrt{\pi}\mu}, \quad g_w(\tilde{x}_-) = \frac{7+18\tilde{x}_- +7\tilde{x}_-^2}{\sqrt{(5+3\tilde{x}_-)(-3-5\tilde{x}_-)}}\sqrt{1+\tilde{x}_-}, \tag{101}$$

where M_w is supposed to be given and $\hat{x}_+ = x_+/\sqrt{rh}$. Note that $g_w(\tilde{x}_-)$ is a monotonically decreasing function spanning the negative real axis in the admissible range $-1<\tilde{x}_-<-3/5$, so that Eq. (100) admits a unique solution in terms of $\tilde{x}_-$ for each values of the positive quantities $\hat{x}_+$ and M_w.

Finally, the condition (91) on the opening displacement imposed by the wedge can be expressed in the normalized form:

$$\hat{x}_+^2 h_w(\tilde{x}_-) = 1, \tag{102}$$

with

$$\begin{aligned} h_w(\tilde{x}_-) = &-\frac{1}{120}\frac{\sqrt{1-\tilde{x}_-}}{(1+\tilde{x}_-)^2}\{2\sqrt{1+\tilde{x}_-}[2(1-\tilde{x}_-)(17+22\tilde{x}_- +17\tilde{x}_-^2)E(\kappa) \\ &+(5+3\tilde{x}_-)(1+26\tilde{x}_- +13\tilde{x}_-^2)K(\kappa)]+(3+67\tilde{x}_- +63\tilde{x}_-^2+25\tilde{x}_-^3)\sqrt{-5-3\tilde{x}_-}\}, \\ \kappa = &(3+5\tilde{x}_-)/(8(1+\tilde{x}_-)). \end{aligned} \tag{103}$$

where, similarly to the previous condition, $h_w(\tilde{x}_-)$ is now a positive monotonically decreasing real function of $\tilde{x}_-$ spanning the positive real axis in the admissible range $-1<\tilde{x}_-<-3/5$. Thus Eq. (102) admits a unique solution in terms of $\tilde{x}_-$ for each value of the positive quantity $\hat{x}_+$.

Further, using Eqs. (100) and (102) we can eliminate $\hat{x}_+$ and find $\tilde{x}_-$ numerically from the obtained relation:

$$f_w(\tilde{x}_-) = \frac{h_w(\tilde{x}_-)}{[-g_w(\tilde{x}_-)]^{4/3}} = \left[\frac{-\Omega(v)}{M_w}\right]^{4/3}. \tag{104}$$

After this x_+ is found from Eq. (102) as

$$\hat{x}_+ = h_w(\tilde{x}_-)^{-1/2}. \tag{105}$$

Then, the stresses for $x_-<x<x_+$ and for $x>x_c$ are

$$\begin{aligned} \sigma_{yy}(x) &= \frac{\mu\Omega(v)}{r}\frac{\sqrt{2(x_+ +x_-)}}{x_+ -x_-}\sqrt{\frac{(x_+ -x)(x-x_-)}{x_c-x}}f_1(x), \\ \sigma_{yy}(x) &= \frac{\mu\Omega(v)}{r}\frac{\sqrt{2(x_+ +x_-)}}{(x_+ -x_-)\sqrt{x_c-x}}\left[\sqrt{(x-x_+)(x-x_-)}f_1(x)-xf_2(x)\right], \end{aligned} \tag{106}$$

respectively, where

$$f_1(x) = x-\frac{(x_+ -x_-)^2}{4(x_+ +x_-)} \quad \text{and} \quad f_2(x) = x-\frac{3x_+^2+2x_+x_-+3x_-^2}{4(x_+ +x_-)}. \tag{107}$$

The total vertical force in each separated wedge contact area and its position are

$$\begin{aligned} Q_y &= \int_{x_-}^{x_+}\sigma_{yy}(x)\,dx = -\frac{\pi}{4}\frac{\mu\Omega(v)}{r}(x_+^2+4x_+x_-+x_-^2), \\ x_Q &= \frac{(x_+ +x_-)(x_+ +3x_-)(3x_+ +x_-)}{4(x_+^2+4x_+x_-+x_-^2)}, \end{aligned} \tag{108}$$

respectively. In addition, the total driving force P is given by

$$P = -2\int_{x_-}^{x_+}\sigma_{yy}(x)u_y'(x)\,dx = -\frac{\mu\Omega(v)}{r^2}\frac{\pi(x_+ +x_-)}{8}(x_+ +3x_-)(3x_+ +x_-) \tag{109}$$

and it can be compared with the energy release rate $G=K_I^2/(2\mu\Omega(v))$, that assumes the approximate form

$$G = -\frac{\mu\Omega(v)}{r^2}\frac{\pi(x_+ +x_-)}{8}\frac{(7x_+ +18x_+x_- +7x_-^2)^2}{(5x_+ +3x_-)(3x_+ +5x_-)} \tag{110}$$

and the exact one

$$G_{Ex} = \frac{\mu\Omega(v)}{r^2}\frac{(x_c-x_-)^2}{9\pi}\left[K\left(\frac{x_+ -x_-}{x_c-x_-}\right)(2x_c+x_-)-E\left(\frac{x_+ -x_-}{x_c-x_-}\right)(2x_c+2x_--x_+)\right]^2. \tag{111}$$

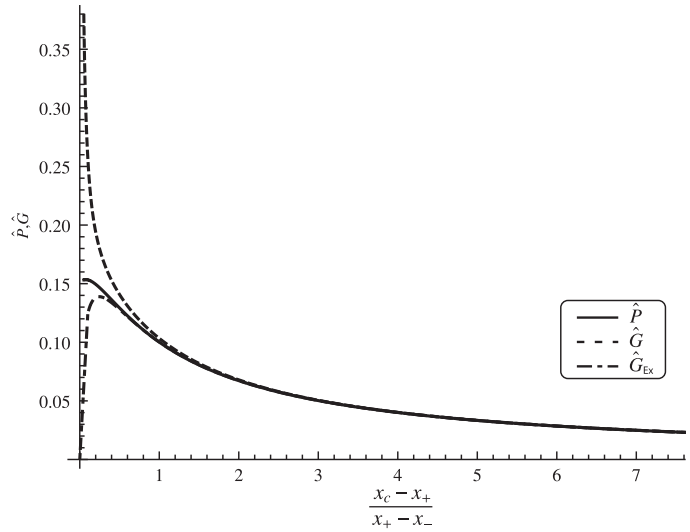

Fig. 9. The driving force as a function of the normalized crack-tip distance, $(x_c-x_+)/(x_+-x_-)$. The exact solution $\hat{G}_{Ex}=G_{Ex}r^2/(\mu\Omega(\nu))$ (111), the approximate solutions $\hat{P}=Pr^2/(\mu\Omega(\nu))$ (109) and $\hat{G}=Gr^2/(\mu\Omega(\nu))$ (110). The plot corresponds to Poisson's ratio equal to 1/3 ($c_1=2c_2$).

Results (109)–(111) are compared in Fig. 9, where they are given as functions of the relative crack-tip distance $(x_c-x_+)/(x_+-x_-)$. The comparative analysis shows the precision of the approximation and the fact that, except when $x_c\to x_+$ the driving force decreases at increasing distance of the crack tip, as expected on physical ground.

The nonzero displacement derivative is

$$\begin{aligned} u_y'(x) &= \frac{1}{r}\frac{\sqrt{2(x_+ + x_-)}}{x_+ - x_-}\frac{1}{\sqrt{x_c - x}}\left[-\sqrt{(x_+ - x)(x_- - x)}f_1(x) - xf_2(x)\right] \quad (x < x_-),\\ &= \frac{x}{r} \quad (x_- < x < x_+),\\ &= \frac{1}{r}\frac{\sqrt{2(x_+ + x_-)}}{x_+ - x_-}\frac{1}{\sqrt{x_c - x}}\left[\sqrt{(x - x_+)(x - x_-)}f_1(x) - xf_2(x)\right] \quad (x_+ < x < x_c). \end{aligned} \tag{112}$$

Finally, the displacement $u_y(x)$ takes the form:

$$\begin{aligned} u_y(x) &= \frac{x_-^2}{2r} + \frac{1}{15}\frac{1}{\sqrt{2(x_+ - x_-)}}\frac{1}{x_+ - x_-}\left[g_+(x) - g_+(x_-)\right] \quad (x < x_-),\\ &= x^2/2r \quad (x_- < x < x_+), = \frac{x_+^2}{2r} + \frac{1}{15}\frac{1}{\sqrt{2(x_+ - x_-)}}\frac{1}{x_+ - x_-}[g_-(x) - g_-(x_+)] \quad (x_+ < x < x_c), \end{aligned} \tag{113}$$

where

$$\begin{aligned} g_\pm(x) &= \sqrt{x_c - x}[12x^2(x_+ + x_-) - (x + 2x_c)(5x_+^2 - 2x_+x_- + 5x_-^2)\\ &\quad \pm \sqrt{(x_- - x)(x_+ - x)}(12x(x_+ + x_-) + x_+^2 + 14x_+x_- + x_-^2)]\\ &\quad - \sqrt{(x_c - x)}(x_+ - x_-)(13x_+^2 + 26x_+x_- + x_-^2)F[\arcsin(\chi(x)), \chi^{-2}(x_+)]\\ &\quad + \sqrt{(x_c - x)}\frac{(x_+ - x_-)^2}{4(x_+ + x_-)}(17x_+^2 + 22x_+x_- + 17x_-^2)E[\arcsin(\chi(x)), \chi^{-2}(x_+)],\\ \chi(x) &= \sqrt{(x_c - x)/(x_c - x_-)}, \end{aligned} \tag{114}$$

with $F(\phi,m)=\int_0^\phi(1-m\sin^2\theta)^{-1/2}\mathrm{d}\theta$ and $E(\phi,m)=\int_0^\phi(1-m\sin^2\theta)^{1/2}\mathrm{d}\theta$ the incomplete elliptic integral of the first and second kind, respectively.

In Figs. 10 and 7 results are shown for $(-\Omega(\nu)/M_w)^{4/3}=2.5$. Eqs. (104) and (105) yield

$$\tilde{x}_- = -0.894, \quad \hat{x}_+ = 0.872, \quad (\hat{x}_- = x_-/\sqrt{rh} = -0.779,\ \hat{x}_c = x_c/\sqrt{rh} = 3.723) \tag{115}$$

such that

$$\tilde{x}_c = x_c/x_+ = 4.269, \quad (x_c - x_+)/(x_+ - x_-) = 1.726 \tag{116}$$

in Fig. 8 and in Fig. 9, respectively.

Distribution of the traction $\sigma_{yy}(x)$ is given in Fig. 10, whereas the deformed contour is represented in Fig. 7. We note that conditions (a) and (b) in (1) are fully respected. In particular, a compressive stress is present in the contact zone and there is no interpenetration between the wedge and the elastic material. The absence of stress singularity at the ends of the contact zone is associated to the continuity of u_y'. The presence of the crack tip and the constraint $u=0$ in the crack continuation line induce a stress distribution which is nonsymmetric with respect to $x=0$ and the consequent existence of

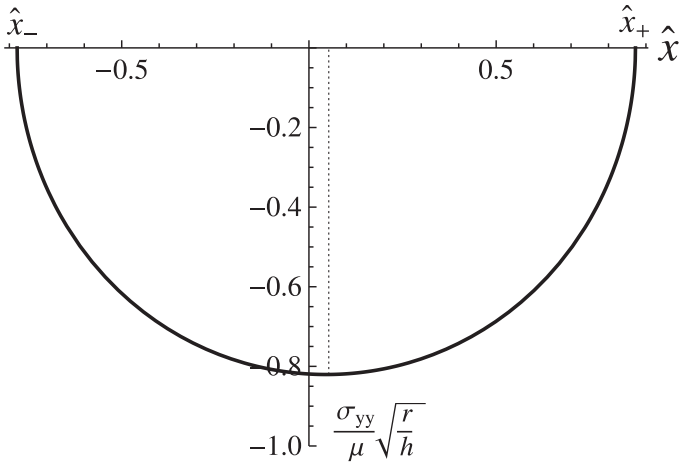

Fig. 10. Distribution of the normalized stress, $\sigma_{yy}/\mu\sqrt{r/h}$, as a function of $\hat{x}=x/\sqrt{rh}$, where $\hat{x}_+=x_+/\sqrt{rh}$ and $\hat{x}_-=x_-/\sqrt{rh}$. Results are given for Poisson's ratio equal to 1/3 and $(-\Omega(\nu)/M_w)^{4/3}=2.5$ (104), which corresponds to $\tilde{x}_c=x_c/x_+=4.269$.

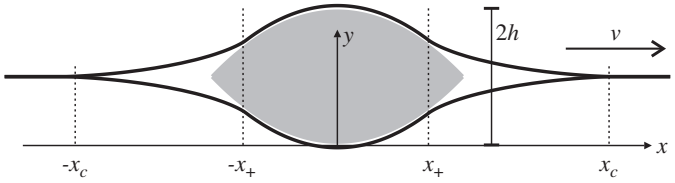

Fig. 11. The wedge moving between two prestress elastic half-planes, $v<c_R$.

the driving force $P=G$. It should be stressed that the driving force is generated by the crack resistance but not by the contact interaction, consistently with Fig. 9.

5. Wedge moving in the interface between two elastic half-planes compressed together

The plane problem for the motion of a rigid wedge through the interface of two elastic half-planes compressed at infinity by a uniform stress $\sigma_{yy}=-\sigma_0<0$ is studied. As for the previous wedge problem, we consider the steady-state movement of a finite-length rigid indenter in the sub-Rayleigh regime.

The wedge is assumed symmetric relatively to both the longitudinal axis, $y=h$, and the normal y-axis, $y(-x,0)=y(x,0)$, $y(\pm x,2h)=2h-y(x,0)$. We also assume that the deformed half-plane boundaries possess the same symmetry in the considered sub-Rayleigh speed regime. Denote the wedge contact region and the half-plane contact region ends as shown in Fig. 11. The wedge–half-plane boundaries' configuration is assumed to consist of five regions, three regions where the displacement is given and two regions where the stresses are given. Namely, with refer to the conditions (a) and (b) in (1), the boundary conditions for the lower half-plane are

$$u_y(x)=y(x)\ (|x|\le x_+),\quad u_y(x)=0\ (|x|\ge x_c),$$
$$\sigma_{yy}=0\ (x_+\le|x|\le x_c),\quad \sigma_{yy}\to-\sigma_0\ (|x|\to\infty) \tag{117}$$

and the symmetric conditions are valid for the upper half-plane.

Representation (85) is used for the displacement derivative and the normal traction, and the following analytical function is introduced:

$$\Phi(\zeta)=\Psi(\zeta)\phi(\zeta),\quad \Psi(\zeta)=\sqrt{(\zeta^2-x_+^2)(\zeta^2-x_c^2)},\ \zeta=x+\mathrm{i}\varepsilon\ (\varepsilon>0), \tag{118}$$

where

$$\Psi(x)=\begin{cases}\sqrt{(x^2-x_+^2)(x^2-x_c^2)} & (|x|>x_c),\\ \mathrm{i}\ \mathrm{sign}\ x\sqrt{(x^2-x_+^2)(x_c^2-x^2)} & (x_+<|x|<x_c),\\ -\sqrt{(x_+^2-x^2)(x_c^2-x^2)} & (|x|<x_+).\end{cases} \tag{119}$$

Outside the contact region $\Re\Phi(x)=0$, and the function $\Phi(\zeta)$ is now defined as

$$\Phi(\zeta)=\frac{\mathrm{i}}{\pi}\int_{-x_+}^{x_+}\frac{y'(\xi)\sqrt{(x_+^2-\xi^2)(x_c^2-\xi^2)}}{\xi-\zeta}\,\mathrm{d}\xi+\mathrm{i}(C_1+C_2\zeta^2). \tag{120}$$

Note that the latter term, $C_2\zeta^2$, reflects the prestress, whereas the linear term is not present due to the symmetry of the problem.

Now consider the stress at remote points and the stress intensity at contact end points. It follows from (85) and (120) that

$$\begin{aligned}
&\sigma_{yy}(x)\sim-\mu\Omega(v)C_2\ \ (x\to\infty),\\
&\sigma_{yy}(x)\sim-\frac{\mu\Omega(v)}{\sqrt{2x_+(x_c^2-x_+^2)(x_+-x)}}\times\left[\frac{1}{\pi}\int_{-x_+}^{x_+}y'(\xi)\sqrt{\frac{(x_++\xi)(x_c^2-\xi^2)}{x_+-\xi}}\,\mathrm{d}\xi-(C_1+C_2x_+^2)\right]\ \ (x\to x_+-0),\\
&\sigma_{yy}(x)\sim\frac{\mu\Omega(v)}{\sqrt{2x_c(x_c^2-x_+^2)(x-x_c)}}\times\left[\frac{1}{\pi}\int_{-x_+}^{x_+}y'(\xi)\sqrt{\frac{(x_c+\xi)(x_+^2-\xi^2)}{x_c-\xi}}\,\mathrm{d}\xi-(C_1+C_2x_c^2)\right]\ \ (x\to x_c+0),
\end{aligned} \tag{121}$$

The conditions in (117) lead to the following equalities:

$$\begin{aligned}
&C_2=\frac{\sigma_0}{\mu\Omega(v)},\\
&C_1=\frac{2}{\pi}\int_0^{x_+}y'(\xi)\sqrt{\frac{x_c^2-\xi^2}{x_+^2-\xi^2}}\xi\,\mathrm{d}\xi-\frac{\sigma_0}{\mu\Omega(v)}x_+^2,\\
&\frac{2}{\pi}\int_0^{x_+}y'(\xi)\sqrt{\frac{x_+^2-\xi^2}{x_c^2-\xi^2}}\xi\,\mathrm{d}\xi+\frac{\sigma_0}{\mu\Omega(v)}(x_c^2-x_+^2)=0.
\end{aligned} \tag{122}$$

As for the previous wedge case, the condition concerning the wedge maximal width must be taken into account and Eq. (91) must be satisfied.

From (122) the different expressions for the contact stresses suitable for $|x|\le x_+$ and $|x|\ge x_c$ are

$$\sigma_{yy}(x)=-\sqrt{\frac{x_+^2-x^2}{x_c^2-x^2}}\left[\sigma_0-\frac{2\mu\Omega(v)}{\pi}V\cdot p\cdot\int_0^{x_+}\sqrt{\frac{x_c^2-\xi^2}{x_+^2-\xi^2}}\frac{y'(\xi)\xi\,\mathrm{d}\xi}{\xi^2-x^2}\right] \tag{123}$$

and

$$\sigma_{yy}(x)=-\sqrt{\frac{x^2-x_c^2}{x^2-x_+^2}}\left[\sigma_0+\frac{2\mu\Omega(v)}{\pi}\int_0^{x_+}\sqrt{\frac{x_+^2-\xi^2}{x_c^2-\xi^2}}\frac{y'(\xi)\xi\,\mathrm{d}\xi}{x^2-\xi^2}\right], \tag{124}$$

respectively. Each of these relations can be analytically continued from one region to the others, and one expression appears equal to the other due to the last condition in (122). From the latter representation in (124) it follows that the analytical function $\phi(\zeta)$ can be represented as

$$\phi(\zeta)=\mathrm{i}\sqrt{\frac{\zeta^2-x_c^2}{\zeta^2-x_+^2}}\left[\frac{\sigma_0}{\mu\Omega(v)}+\frac{2}{\pi}\int_0^{x_+}\sqrt{\frac{x_+^2-\xi^2}{x_c^2-\xi^2}}\frac{y'(\xi)\xi\,\mathrm{d}\xi}{\zeta^2-\xi^2}\right] \tag{125}$$

and this yields

$$u_y'(x)=-\sqrt{\frac{x_c^2-x^2}{x^2-x_+^2}}\left[\frac{\sigma_0}{\mu\Omega(v)}+\frac{2}{\pi}\int_0^{x_+}\sqrt{\frac{x_+^2-\xi^2}{x_c^2-\xi^2}}\frac{y'(\xi)\xi\,\mathrm{d}\xi}{x^2-\xi^2}\right]\operatorname{sign}x\quad(x_+\le|x|\le x_c). \tag{126}$$

The unknown values x_+ and x_c are defined by Eq. (91) and the last condition in (122).

5.1. The parabolic wedge

For this shape we consider the solution independently. When the shape of the indenter at the contact zone is parabolic the condition in (121) of zero stress intensity at x_+ gives

$$C_1=-x_+^2\left\{\frac{2x_+}{3\pi r}\tilde{x}_c\left[(\tilde{x}_c^2-1)K(\tilde{x}_c^{-2})-(\tilde{x}_c^2-2)E(\tilde{x}_c^{-2})\right]+\frac{\sigma_0}{\mu\Omega(v)}\right\}, \tag{127}$$

where $\tilde{x}_c = x_c/x_+$. The condition (121) of zero stress intensity at x_c takes the form

$$x_+^2(\tilde{x}_c^2-1)\left\{\frac{2x_+}{\pi r}\tilde{x}_c[K(\tilde{x}_c^{-2})-E(\tilde{x}_c^{-2})]+\frac{\sigma_0}{\mu\Omega(\nu)}\right\}=0, \tag{128}$$

where the solution $\tilde{x}_c = 1$ is associated with tensile stress in the region $|x| < x_+$ and it cannot be accepted. Then, Eq. (128) can be given the equivalent normalized form

$$\Omega(\nu)\hat{x}_+ g_p(\tilde{x}_c) = M_p, \tag{129}$$

where

$$\hat{x}_+ = \frac{x_+}{\sqrt{rh}}, \quad g_p(\tilde{x}_c) = \frac{2\tilde{x}_c}{\pi}[E(\tilde{x}_c^{-2})-K(\tilde{x}_c^{-2})], \quad M_p = \frac{\sigma_0}{\mu}\sqrt{\frac{r}{h}} \tag{130}$$

and $g_p(\tilde{x}_c)$ is a monotonic increasing real function of $\tilde{x}_c$ spanning the negative real axis in the admissible range $1 < \tilde{x}_c < \infty$, so that Eq. (129) admits a unique solution in term of $\tilde{x}_c$ for each value of the positive quantities $\hat{x}_+$ and M_p.

Lastly, condition (91) is represented in the normalized form

$$\hat{x}_+^2 h_p(\tilde{x}_c) = 1, \tag{131}$$

where

$$h_p(\tilde{x}_c) = 1+\frac{2}{\pi}\left\{-\frac{1}{\tilde{x}_c}\int_{-1}^{1}\sqrt{\frac{\tilde{x}_c^2-\xi^2}{1-\xi^2}}\Pi\left(-\frac{\tilde{x}_c^2-1}{\tilde{x}_c^2}\frac{\xi^2}{1-\xi^2},\frac{\tilde{x}_c^2-1}{\tilde{x}_c^2}\right)\mathrm{d}\xi+2K\left(\frac{\tilde{x}_c^2-1}{\tilde{x}_c^2}\right)K\left(\tilde{x}_c^{-2}\right)-2\tilde{x}_c^2E\left(\frac{\tilde{x}_c^2-1}{\tilde{x}_c^2}\right)\left[K\left(\tilde{x}_c^{-2}\right)-E\left(\tilde{x}_c^{-2}\right)\right]\right\} \tag{132}$$

and $\Pi(n,m) = \int_0^{\pi/2}(1-n\sin^2\theta)^{-1}(1-m\sin^2\theta)^{-1/2}\mathrm{d}\theta$ is the complete elliptic integral of the third kind. Note that the integral in Eq. (132) has been computed numerically and that $h_p(\tilde{x}_c)$ is a monotonic increasing function of $\tilde{x}_c$ spanning the positive real axis in the admissible range $1 < \tilde{x}_c < \infty$, so that Eq. (131) admits a unique solution in terms of $\tilde{x}_c$ for each value of the quantity $\hat{x}_+$.

Similarly to Section 4.1, a solution of Eqs. (129) and (131) can be found numerically. We define

$$f_p(\tilde{x}_c) = \frac{h_p(\tilde{x}_c)}{g_p(\tilde{x}_c)^2} = \left(\frac{\Omega(\nu)}{M_p}\right)^2 \tag{133}$$

in terms of $\tilde{x}_c$, where M_p is a given quantity, and compute $\hat{x}_+$ as

$$\hat{x}_+ = h_p(\tilde{x}_c)^{-1/2}. \tag{134}$$

Then, the nonzero stresses for $|x| < x_+$ and $|x| > x_c$ are

$$\begin{aligned}\frac{\sigma_{yy}(\tilde{x})}{\sigma_0} &= \sqrt{\frac{1-\tilde{x}^2}{\tilde{x}_c^2-\tilde{x}^2}}\left\{1+\frac{K(\tilde{x}_c^{-2})\tilde{x}^2-E(\tilde{x}_c^{-2})\tilde{x}_c^2+\Re\Pi(\tilde{x}^{-2},\tilde{x}_c^{-2})(\tilde{x}_c^2-\tilde{x}^2)}{\tilde{x}_c^2[K(\tilde{x}_c^{-2})-E(\tilde{x}_c^{-2})]}\right\}\\ &= -\sqrt{\frac{\tilde{x}^2-1}{\tilde{x}^2-\tilde{x}_c^2}}\left\{1-\frac{K(\tilde{x}_c^{-2})\tilde{x}^2-E(\tilde{x}_c^{-2})\tilde{x}_c^2-\Pi(\tilde{x}^{-2},\tilde{x}_c^{-2})(\tilde{x}^2-\tilde{x}_c^2)}{\tilde{x}_c^2[K(\tilde{x}_c^{-2})-E(\tilde{x}_c^{-2})]}\right\},\end{aligned} \tag{135}$$

respectively, where $\tilde{x} = x/x_+$. The stress distribution is reported in Fig. 12 for $M_p = 0.122$, $\tilde{x}_c = 3.000$, $\hat{x}_+ = 0.703$.

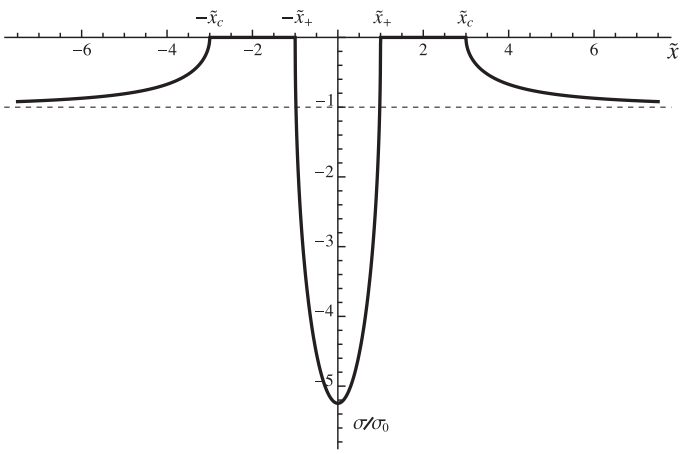

Fig. 12. Distribution of the normalized contact stresses σ_{yy}/σ_0, as a function of $\tilde{x} = x/x_+$ for $M_p = 0.122$, $\tilde{x}_c = 3.000$.

Finally, the displacements are

$$\frac{u_y(\tilde{x})}{x_+^2/2r}=\tilde{x}^2\ (|x|<x_+),\quad \frac{u_y(\tilde{x})}{x_+^2/2r}=\tilde{x}_c\ (|x|>x_c),$$

$$\frac{u_y(\tilde{x})}{x_+^2/2r}=1+\frac{2}{\pi}\left\{2E(\tilde{x}_c^{-2})F\left[\arcsin\left(\frac{\tilde{x}_c\sqrt{\tilde{x}^2-1}}{\tilde{x}\sqrt{\tilde{x}_c^2-1}}\right),\frac{\tilde{x}_c^2-1}{\tilde{x}_c^2}\right]-\frac{1}{\tilde{x}_c}L(\tilde{x},\tilde{x}_c)\right.$$

$$\left.-2\mathrm{i}\tilde{x}_c[K(\tilde{x}_c^{-2})-E(\tilde{x}_c^{-2})]\left[E(\arcsin(\tilde{x}_c^{-2}),\tilde{x}_c^2)-E\left(\arcsin\left(\frac{\tilde{x}}{\tilde{x}_c}\right),\tilde{x}_c^2\right)\right]\right\}\quad (x_+<|x|<x_c), \tag{136}$$

where

$$L(\tilde{x},\tilde{x}_c)=\int_{-1}^{1}\sqrt{\frac{\tilde{x}_c^2-\xi^2}{1-\xi^2}}\Pi\left[-\frac{(\tilde{x}_c^2-1)\xi^2}{\tilde{x}_c^2(1-\xi^2)},\arcsin\left(\frac{\tilde{x}_c\sqrt{\tilde{x}^2-1}}{\tilde{x}\sqrt{\tilde{x}_c^2-1}}\right),\frac{\tilde{x}_c^2-1}{\tilde{x}_c^2}\right]\mathrm{d}\xi, \tag{137}$$

with $\Pi(n,\phi,m)=\int_0^{\phi}(1-n\sin^2\theta)^{-1}(1-m\sin^2\theta)^{-1/2}\,\mathrm{d}\theta$ the incomplete elliptic integral of the third kind.

Note that there is no driving force, and the wedge moves freely inside the structure with any constant sub-Rayleigh speed.

6. Concluding remarks

In this paper, we have discussed the general conditions under which a body moving in contact with an elastic medium meets zero driving force and presented some examples of resistance-free motion. In addition to the resistance-free sub-Rayleigh speed regimes in the half-plane problem and for the two half-planes compressed, we have found a sharp decrease in the resistance in the vicinity of the longitudinal wave speed, with zero limit at this speed.

We also have examined in detail all the other speed regimes, where a driving force is required to support the motion. In particular, we have derived a general solution of the moving-contact plane problem valid for all speed ranges, $0<v<\infty$, including super-Rayleigh sub- and intersonic speeds (Section 3.1). In the case of a single simply connected contact zone, this solution is presented for a general smooth shape of the indenter. The general expressions are then deduced for the case of symmetry, and then for a parabolic (or a constant curvature) indenter. Also, the dynamic wedging problem is considered for a finite length wedge moving at sub-Rayleigh speed at a distance of the crack tip and within two half-planes compressed together.

In all these cases, we have determined the driving forces caused by the main underlying factors: stress field singular points in the contact region (the super-Rayleigh subsonic regime), wave radiation (the intersonic and supersonic regimes) and crack resistance (the wedging problem). Note that in the latter sub-Rayleigh speed problem, the driving force is equal to the crack resistance, while the contact sliding itself gives no contribution to this force.

The contact problems are considered based on a general solution as the steady-state limit of the corresponding transient problem. In this solution, the stresses and the displacements are expressed through a single analytical function for all speed ranges. The uniqueness is achieved by this limit and by an energy condition. The latter states that energy-source singular points, which can appear in a solution, must be eliminated, and only energy absorbing ones can be accepted.

Based on the conditions allowing the 'paradox' to exist, it is clear that the considered examples do not exhaust the class of structures where such resistance-free motion can exist. In particular, this concerns various 1D models and more complicated 2D and 3D structures. Note that, in the latter case, the Rayleigh waves can be excited by a finite indenter moving with a super-Rayleigh speed along the boundary of an elastic half-space.

The considered problems are studied in the framework of linear elasticity; strains and rotations are assumed to be small except in the vicinity of a singular point. However, the resistance-free motion conditions are valid independently of the elastic medium model, the exact or the linearized one. The only condition for the medium is that the strain energy must be potential (in the nonlinear elasticity terminology an hyperelastic material). In this connection we recall that the energy fluxes can be determined using the Eshelby–Cherepanov–Rice integral over a suitably built contour or surface, applicable for both the exact nonlinear elasticity and the linearized one. Along with this, if the contact strains and rotations are not small enough, the exact formulation may lead to essential changes of the contact area and the contact stress distribution.

Acknowledgments

This paper was written when L.I. Slepyan was a Visiting Professor at Cagliari University under the 2011 program funded by Regione Autonoma della Sardegna. L.I. is also thankful for the support provided by FP7-People-2011-IAPP European Union Grant no. 284544.

References

Barenblatt, G.I., Cherepanov, G.P., 1960. On the wedging of brittle bodies. Prikl. Mat. Mekh. 24 (4), 667–682. (in Russian); J. Appl. Math. Mech. (PMM), 24(4), 993–1014 (English Translation).

Barenblatt, G.I., Goldstein, R.V., 1972. Wedging of an elastic body by a slender wedge moving with a constant super-Rayleigh subsonic velocity. Int. J. Fract. Mech. 8 (4), 427–434.

Broberg, K.B., 1999. Cracks and Fracture. Academic Press, London.

Brock, L.M., 2002. Exact analysis of dynamic sliding indentation at any constant speed on an orthotropic or transversely isotropic half-space. ASME J. Appl. Mech. 69, 340–345.

Cagniard, L., 1962. Reflection and Refraction of Progressive Seismic Waves. McGraw-Hill (Translated from Cagniard (1939)).

Comninou, Maria, Dundurs, J., 1977. Elastic interface waves involving separation. ASME J. Appl. Mech. 44, 222–226.

Craggs, J.W., Roberts, A.M., 1967. On the motion of a heavy cylinder over the surface of an elastic half-space. ASME J. Appl. Mech. 34, 207–209.

Darrigol, O., 2002. Between hydrodynamics and elasticity theory: the first five births of the Navier–Stokes equation. Arch. Hist. Exact Sci. 56, 95–150.

De Hoop, A.T., 1959. The surface line source problem. Appl. Sci. Res. B 8, 349–356.

Freund, L.B., 1990. Dynamic Fracture Mechanics. Cambridge University Press, Cambridge.

Galin, L.A., Gladwell, G.M.L. (Eds.), 2008. Contact Problems. Springer.

Gao, H., Huang, Y., Abraham, F.F., 2001. Continuum and atomistic studies of intersonic crack propagation. J. Mech. Phys. Solids 49, 2113–2132.

Georgiadis, H.G., Barber, J.R., 1993. On the super-Rayleigh/subsonic elastodynamic indentation problem. J. Elasticity 31, 141–161.

Geubelle, P.H., Kubair, D.V., 2001. Intersonic crack propagation in homogeneous media under shear-dominated loading: numerical analysis. J. Mech. Phys. Solids 49, 571–587.

Huang, Y., Wang, W., Liu, C., Rosakis, A.J., 1998. Intersonic crack growth in bimaterial interfaces: an investigation of crack face contact. J. Mech. Phys. Solids 46, 2233–2259.

Kostrov, B.V., Nikitin, L.V., Flitman, L.M., 1969. Mechanics of brittle fracture. Mech. Solids 3, 112–125.

Needleman, A., 1999. An analysis of intersonic crack growth under shear loading. ASME J. Appl. Mech. 66, 847–857.

Radi, E., Loret, B., 2008. Mode I intersonic crack propagation in poroelastic media. Mech. Mater. 40, 524–548.

Samudrala, O., Huang, Y., Rosakis, A.J., 2002. Subsonic and intersonic mode II crack propagation with a rate-dependent cohesive zone. J. Mech. Phys. Solids 50, 1231–1268.

Slepyan, L.I., 1972. Transient Elastic Waves. Sudostroenie, Leningrad (in Russian).

Slepyan, L.I., 2002. Models and Phenomena in Fracture Mechanics. Springer, Berlin.

Yoffe, E.N., 1951. The moving Griffith crack. Philos. Mag. 42, 739–750.